



ACADIA
CENTRE FOR
ESTUARINE RESEARCH

**SEDIMENT SETTLING RATE ANALYSES
FOR A SEDIMENT STABILITY STUDY OF THE
INNER MIRAMICHI BAY, NEW BRUNSWICK**

**Wolfville, Nova Scotia
Canada**

S045



Prepared For

Public Works Canada
Architectural and Engineering Services
P.O. Box 7350
St. John, New Brunswick
E2L 4J4

Contract No. 2105182

**SEDIMENT SETTLING RATE ANALYSES
FOR A SEDIMENT STABILITY STUDY OF THE
INNER MIRAMICHI BAY, NEW BRUNSWICK**

Prepared By

C.L. Amos
Geological Survey of Canada
Bedford Institute of Oceanography
Dartmouth, Nova Scotia
B2Y 4A2
and
A.J. Gibson and M. Brylinsky
Acadia Centre For Estuarine Research
Acadia University
Wolfville, Nova Scotia
B0P 1H0

June, 1992

Acadia Centre For Estuarine Research Publication No. 23

SEDIMENT SETTLING RATE ANALYSES FOR A SEDIMENT STABILITY STUDY OF THE INNER MIRAMICHI BAY, NEW BRUNSWICK

I. Background and Objectives

As part of a programme to evaluate the physical characteristics and stability of sediments within the Inner Bay of the Miramichi Estuary, settling rate measurements were carried out on four bulk seabed samples collected with a medium Van Veen grab sampler. Samples were taken from the Control Site (Station 1), a 1990 spoils mound at Dump Site B (Station 7), in the area of Reach 22 of the dredged channel (Station 13), and in the area of Reach 20 of the dredged channel (Station 18). The exact location of each sample is documented in Brylinsky *et al.* (1992). Sub-samples from each of the four sites were prepared for a series of settling rate tests at starting suspended sediment concentrations ranging between 2-40 g/L, and at salinities ranging between 13-30‰. These are considered to cover the range of probable conditions prevalent within the Miramichi Inner Bay.

The objectives of this study were: (1) to determine the conditions under which hindered settling and fluid mud generation takes place; and (2) to determine the relationship between mass settling rate and initial sediment concentration and salinity.

II. Methodology

Bulk samples were split and wet sieved through a 64 micron mesh in order to remove the sand fraction. The finer fraction was mixed with seawater to a known starting suspended sediment concentration and then thoroughly mixed within a settling column. The settling column consisted of a 40 cm high, 6 cm dia cylinder, a size previously shown to be free of problems associated with wall effects (Lovell and Rose 1991). Changes in sediment concentration with time were measured by reference to fluid density with a calibrated hydrometer. Hydrometer measures were taken at intervals of 1, 2, 3, 5, 10, 15, 20, 30, 45 and 60 min after initiation of each experiment. The water temperature of each experiment was between 20-22 °C.

III. Results

A total of 119 experiments were carried out: 29 on the Control Site sample, 30 on the Dump Site sample, 30 on the sample from Reach 22, and 30 on the sample from Reach 20. In general, sediment concentration versus time showed an exponential decrease that appeared to be bimodal; an initial rapid drop in concentration within several minutes was followed by a slow rate of settling that took place over several hours. Figures of all time series together with regression analyses of the trends are shown in Appendix I. The inflection point between the two modes of settling is at a constant concentration of circa 4 g/L at initial sediment concentrations (C_0) below 20 g/L. Above 20 g/L the inflection point occurs at approximately twice this value (Figure 1). This indicates that hindered settling and the potential for fluid mud development occurs at $C_0 > 20$ g/L. This inflection point is independent of salinity (Figure 2).

In order to quantify the results two models of sedimentation were tested: (1) a linear model of particle settling through time whereby:

$$C_t = C_0 - k_{lin}t \quad \text{where,}$$

- C_t = Concentration at time t
- C_0 = Concentration at time 0
- k_{lin} = slope
- t = time

and (2) the model of Krone (1962) whereby the still water rate of change in concentration is related to mass settling velocity (V_0) in exponentially decaying form as follows:

$$C_t = C_0 \exp [-ptk_{\log}] \quad \text{where,}$$

C_t	=	Concentration at time t
C_0	=	Concentration at time 0
p	=	probability of particle deposition
t	=	time
k_{\log}	=	slope

The probability of particle deposition (p) for still water is set to 1. k_{\log} is equal to V_0/y (units of 1/s) where y is the depth below the water surface at which V_0 is evaluated. This depth varied, due to changes in water density, between 12 and 17 cm. Nevertheless, we adopted an average of 14 cm throughout this study.

Reasonable fits of the observations to either model could not be achieved by considering the concentration decay as a whole. Much better results were achieved by fitting curves to trends either side of the inflection point. Appendix I presents regression coefficients for both the linear and exponential decay models. The slope of the initial trend is defined as K1 whereas the latter is referred to as K2. Regression coefficients >0.90 were obtained in most instances.

Figures 3-6 illustrate the relationship between C_0 and slope for the linear and exponential decay models. $K1_{lin}$ showed a strong linear relationship to C_0 to about 20 g/L. For the period of initial rapid settling slopes based on the linear model were best correlated to C_0 . Correlation coefficients in excess of 0.88 were thus achieved (Figure 3). A poorer but nevertheless significant fit was also achieved using slopes based on the exponential decay model. For $C_0 < 20$ g/L this model yielded correlation coefficients between 0.12 and 0.83 (Figure 4).

In all but the Reach 22 case, $K1_{lin}$ is small (<-0.5) and apparently constant below 2 g/L. Note the position of the intercept of the best fit lines at circa 2 g/L in Figure 3. This we interpret as the region of floc settling where floes settle independent of other floes in suspension. For a $K1_{lin} = -0.5$ and using the transform of Krone (1972):

$$V_0 = |K1_{lin}|/14 = 0.036 \text{ cm/s}$$

This value of V_0 is very close to values reported by Amos and Mosher (1985) from analysis of suspended sediments from the Bay of Fundy using a bottom withdrawal method.

Between a concentration range of 2-20 g/L we interpret conditions of mass settling. The trends in $K1_{lin}$ between the control site, Dump Site B, and Reach 20 appear to be similar, with $K1_{lin}$ attaining a minimum value on the order of -6 to -7. The Reach 22 sample, by contrast, shows evidence of a generally lower rate of settling at a given starting concentration.

The following are the linear equations describing $K1_{lin}$ as a function of C_0 for the four sites described in this study:

$$\text{Control Site: } K1_{lin} = 1.352 - 0.387(C_0); [2 < C_0 < 20 \text{ g/L}]$$

$$\text{Dump Site B: } K1_{lin} = 0.620 - 0.276(C_0); [2 < C_0 < 20 \text{ g/L}]$$

$$\text{Reach 22: } K1_{lin} = -0.285 - 0.177(C_0); [2 < C_0 < 20 \text{ g/L}]$$

Reach 20: $K_{1\text{lin}} = -0.774 - 0.364(C_0)$; [2 < C_0 < 20 g/L]

Above 20 g/L, $K_{1\text{lin}}$ appeared to remain constant and high. We presume that this represents the beginning of conditions of hindered settling though we note the settling rate is no less than under conditions of mass settling. In all cases where $C_0 > 20$ g/L, $K_{1\text{lin}}$ is equated with its value at 20 g/L.

The period of slow settling was best approximated by a logarithmic model (Appendix 1). The value of K_2 in both the linear and log model was circa -0.03 (Figures 5 and 6). This yielded a mass settling rate of 2.1×10^{-5} m/s.

The direct relationship between settling rate and suspended sediment concentration is clearly seen in Figures 7 to 10. Notice in each case the monotonic decrease in $K_{1\text{lin}}$ with sediment concentration through the mass settling range and the lack of correlation with salinity. This trend breaks down in the region of hindered settling such that $K_{1\text{lin}}$ appears independent of both salinity and concentration. At concentrations >20 g/L, there is a change in the trend of $K_{1\text{lin}}$ with an associated decrease in mass settling rate. This may herald the onset of conditions leading to the development of fluid muds (Wolanski *et al.* 1992).

IV. References

- Amos, C.L. and D.C. Mosher.** 1985. Erosion and deposition of fine-grained sediments from the Bay of Fundy. *Sedimentology* 32:815-832.
- Brylinsky, M., A.J. Gibson, G.R. Daborn, C.L. Amos and H.A. Christian.** 1992. Miramichi Inner Bay Sediment Stability Study. Report to Public Works Canada: Contract No. 2105182. Acadia Centre for Estuarine Research Publication No. 22. Acadia University, Wolfville, Nova Scotia.
- Krone, R.B.** 1962. Flume studies of the transport of sediment in estuarial shoaling processes. *Final rep.* Hydraulic Engineering Laboratory and Sanitary Engineering Research Laboratory, University of California, Berkeley.
- Lovell, C.J. and C.W. Rose.** 1991. The effect of sediment concentration and tube-diameter on particle settling velocity measured beyond Stokes' range: experiments and theory. *Journal of Sedimentary Petrology*. 61(4):583-589.
- Wolanski, E., R.J. Gibbs, Y. Mazda, A. Mehta and B. King.** 1992. The role of turbulence in the settling of mud flocs. *Journal of Coastal Research*. 8(1):35-64.

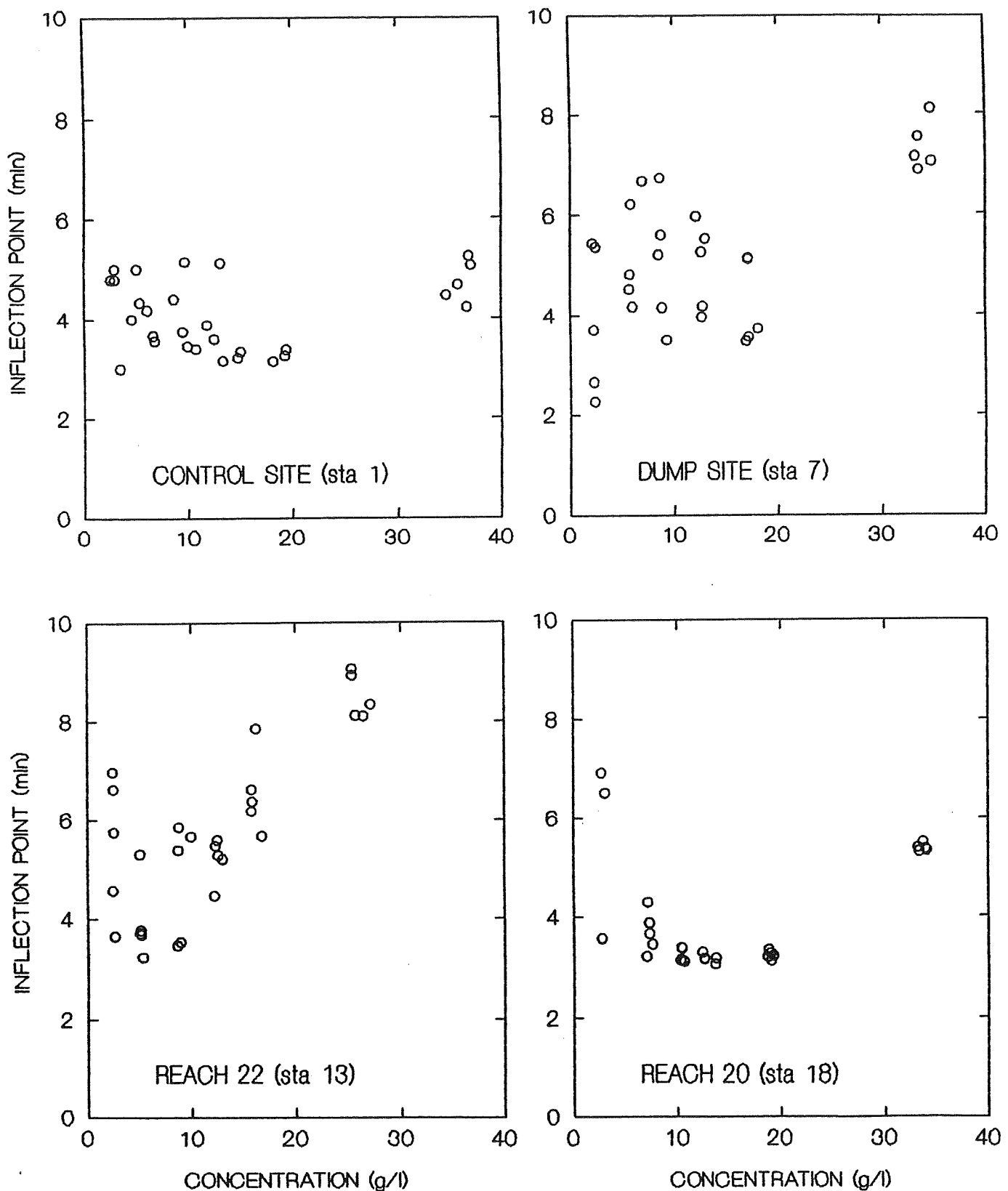


Figure 1. Relationship between initial suspended sediment concentration and the inflection point separating the two modes of settling.

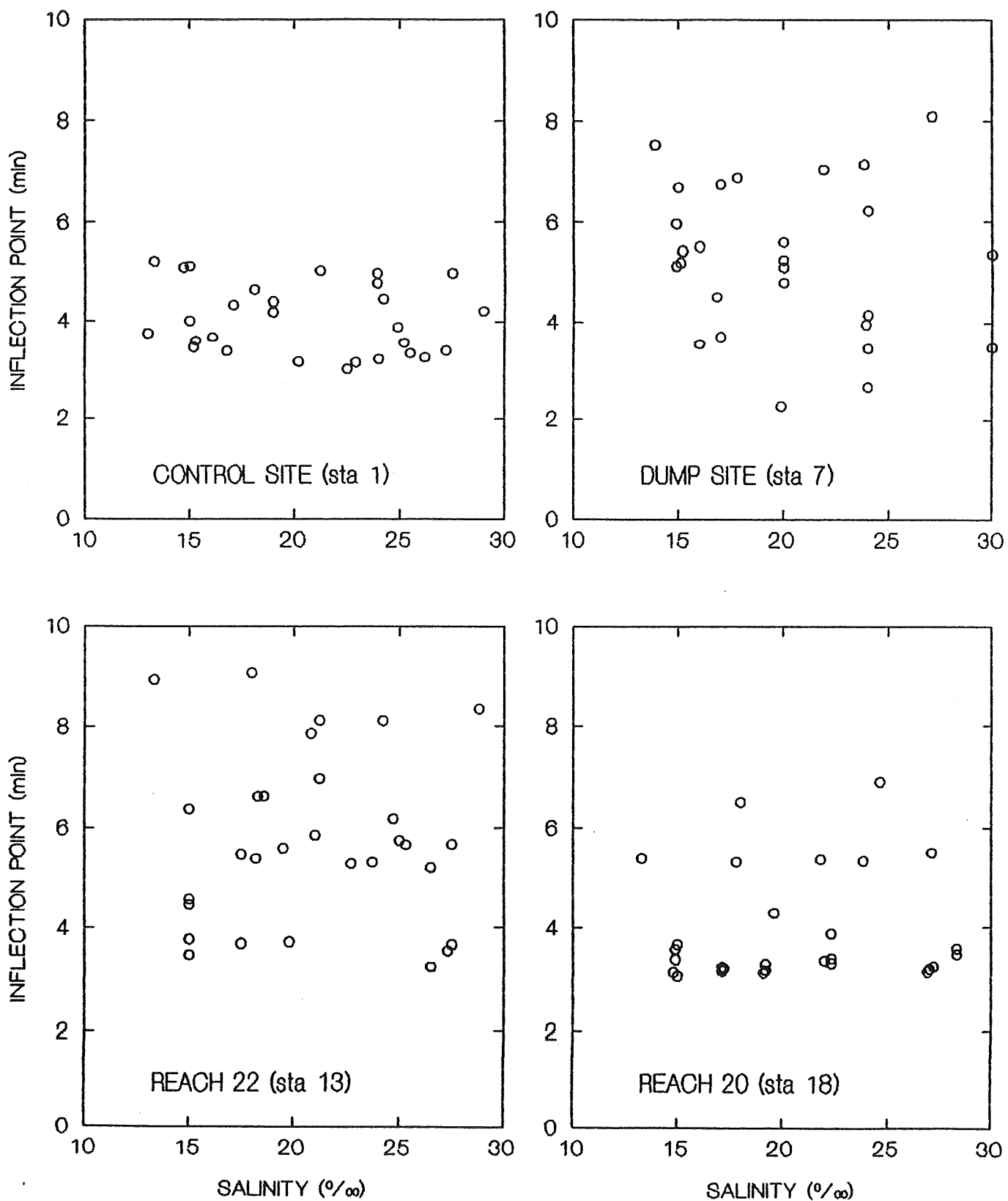


Figure 2. Relationship between salinity and the inflection point separating the two modes of settling.

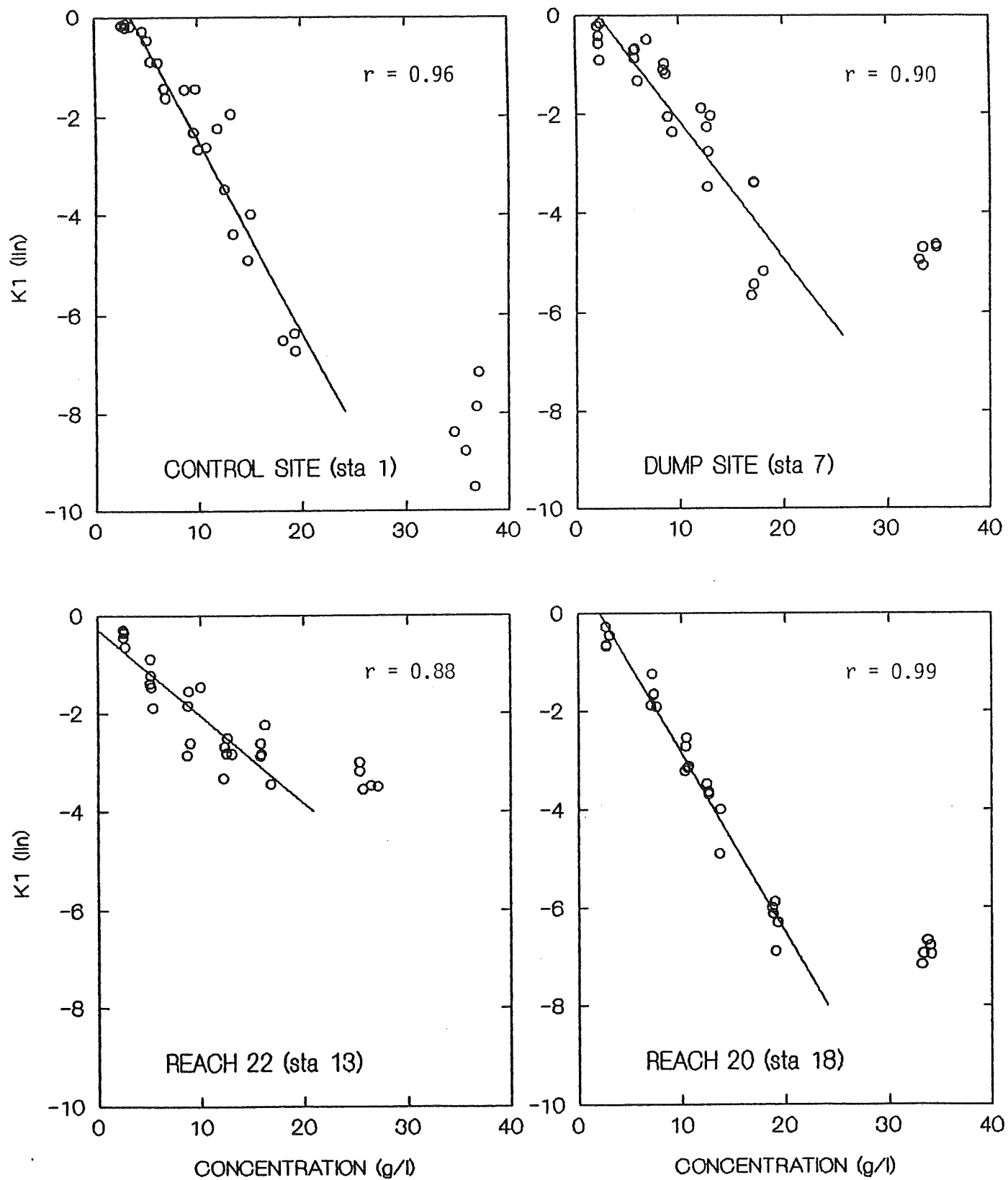


Figure 3. Relationship between $K_1 \text{ (ln)}$ and initial suspended sediment concentration (r^2 values are based on data for $C_0 < 20 \text{ g/L}$).

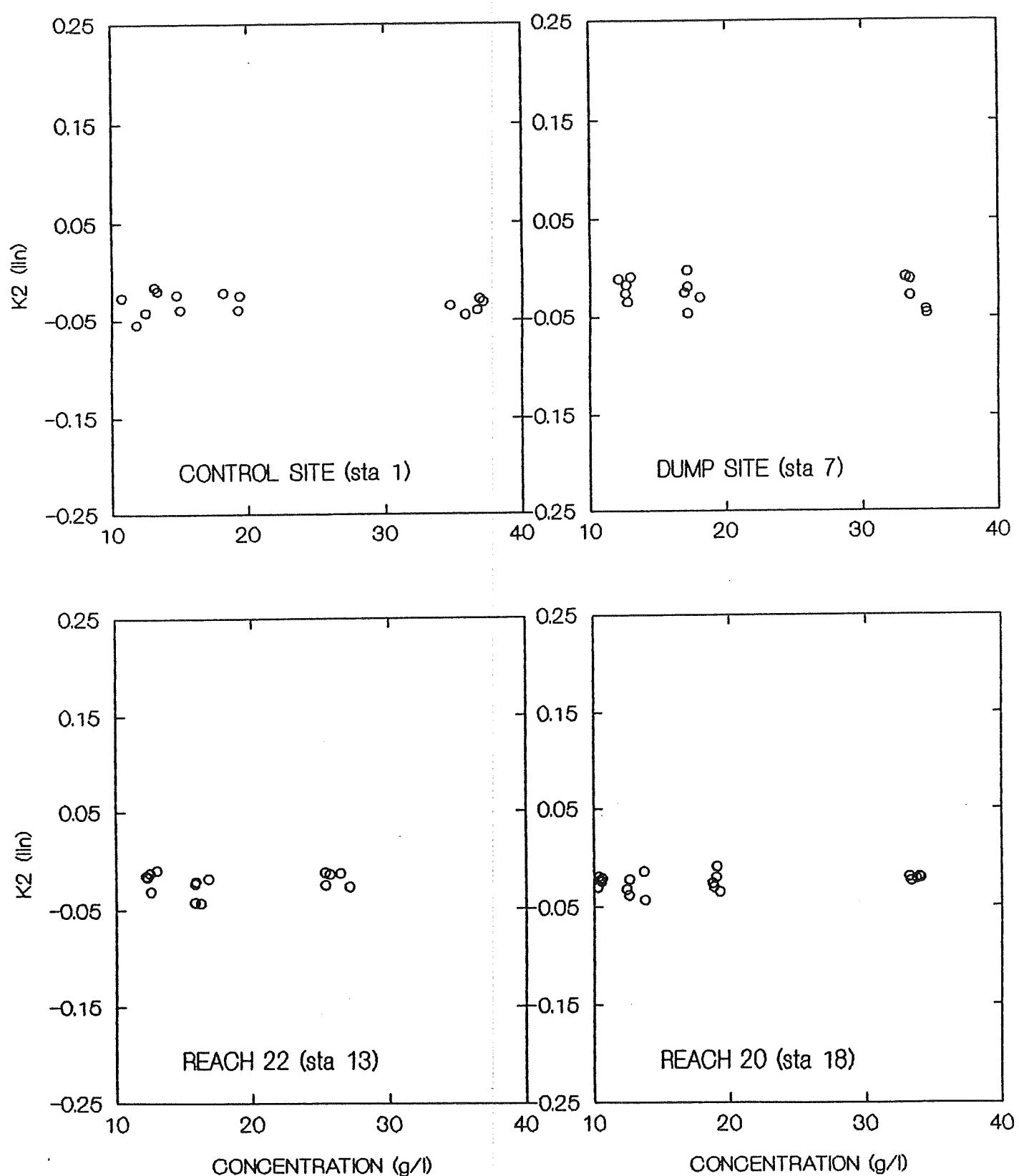


Figure 4. Relationship between $K_2\ln$ and initial suspended sediment concentration.

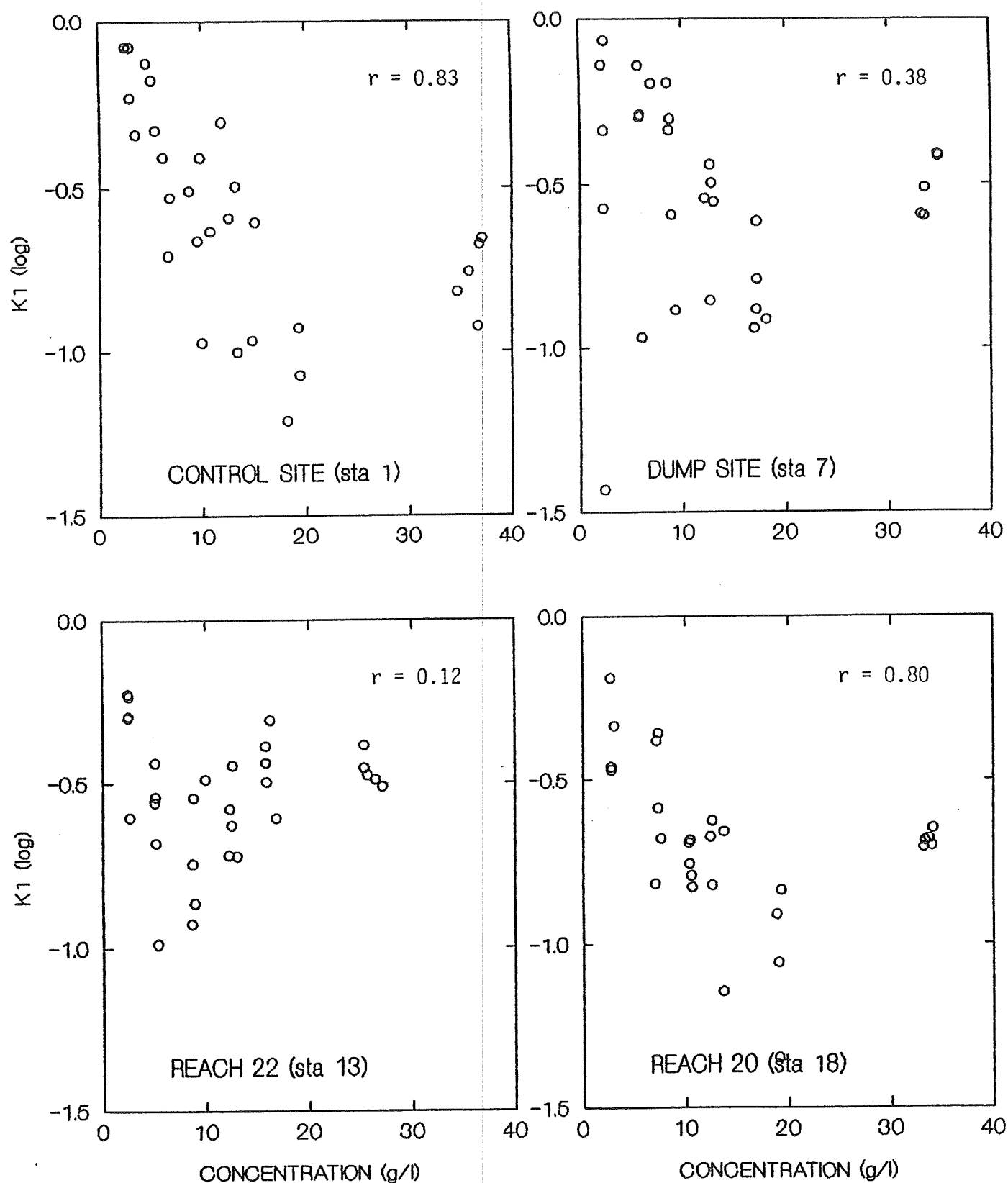


Figure 5. Relationship between $K_2 \text{ log}$ and initial suspended sediment concentration (r^2 values are based on data for $C_0 < 20 \text{ g/L}$).

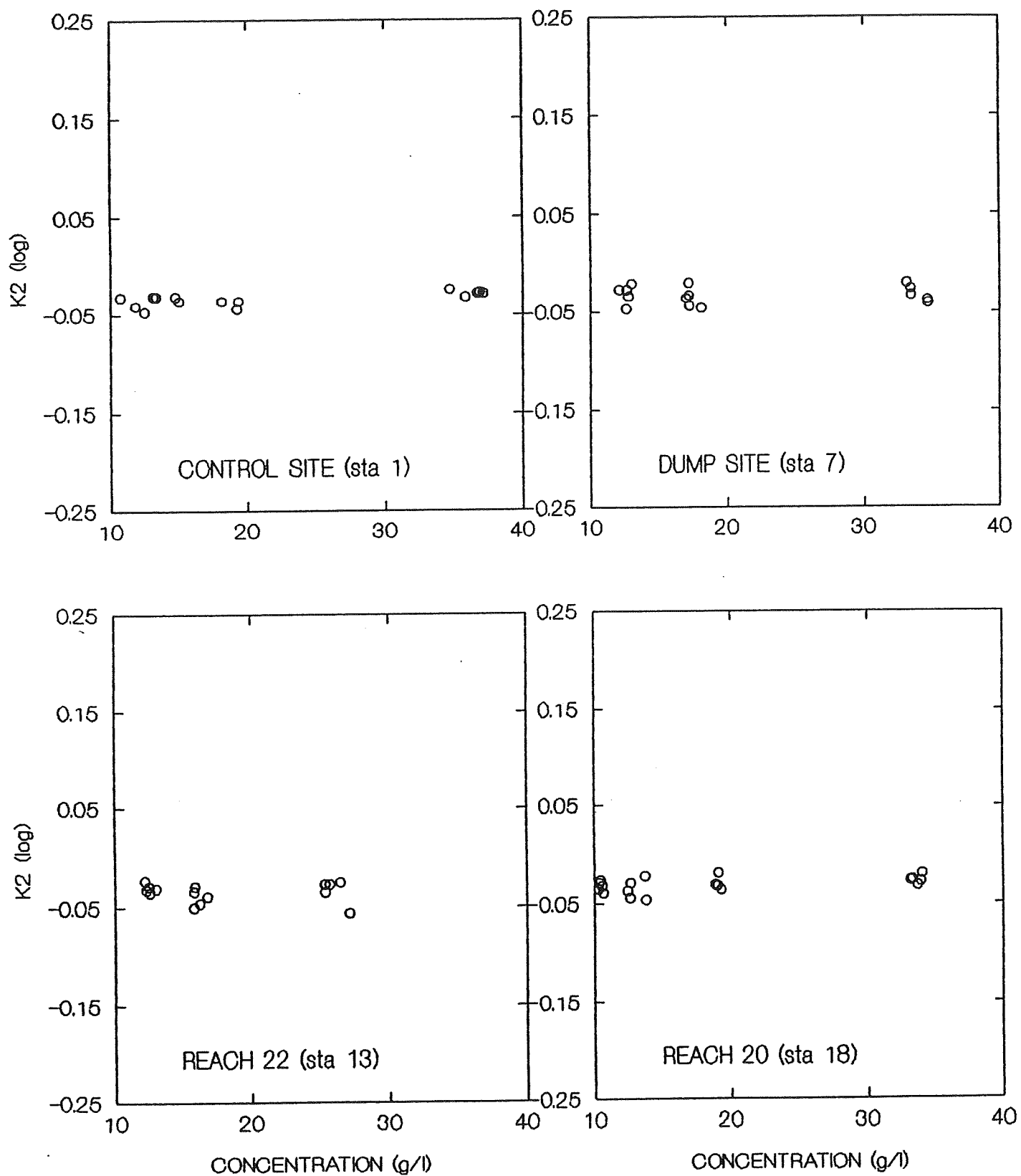


Figure 6. Relationship between $K_2 \log$ and initial suspended sediment concentration.

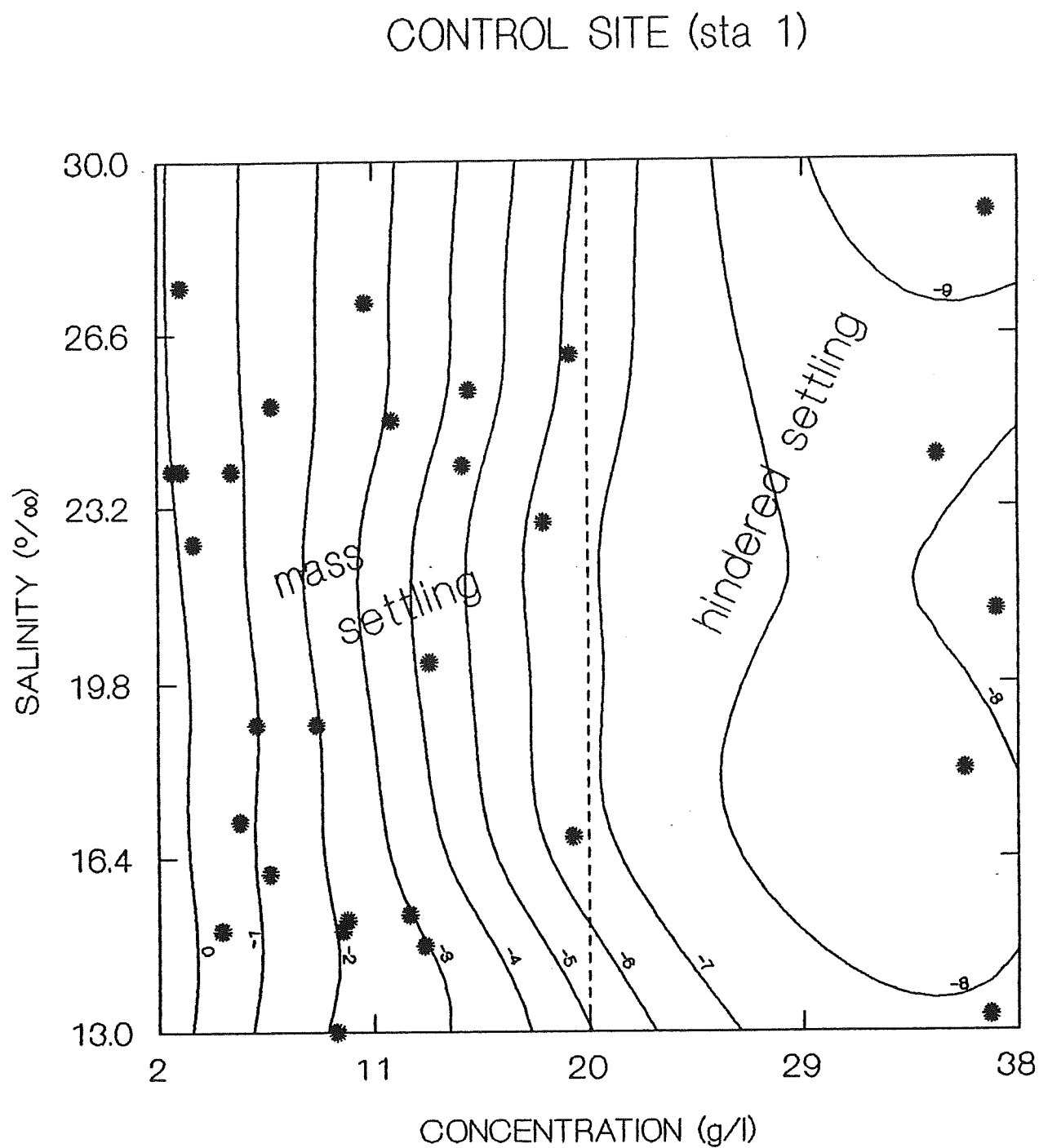


Figure 7. $K_{1\text{lin}}$ as a function of initial suspended sediment concentration and salinity for the Control Site sample.

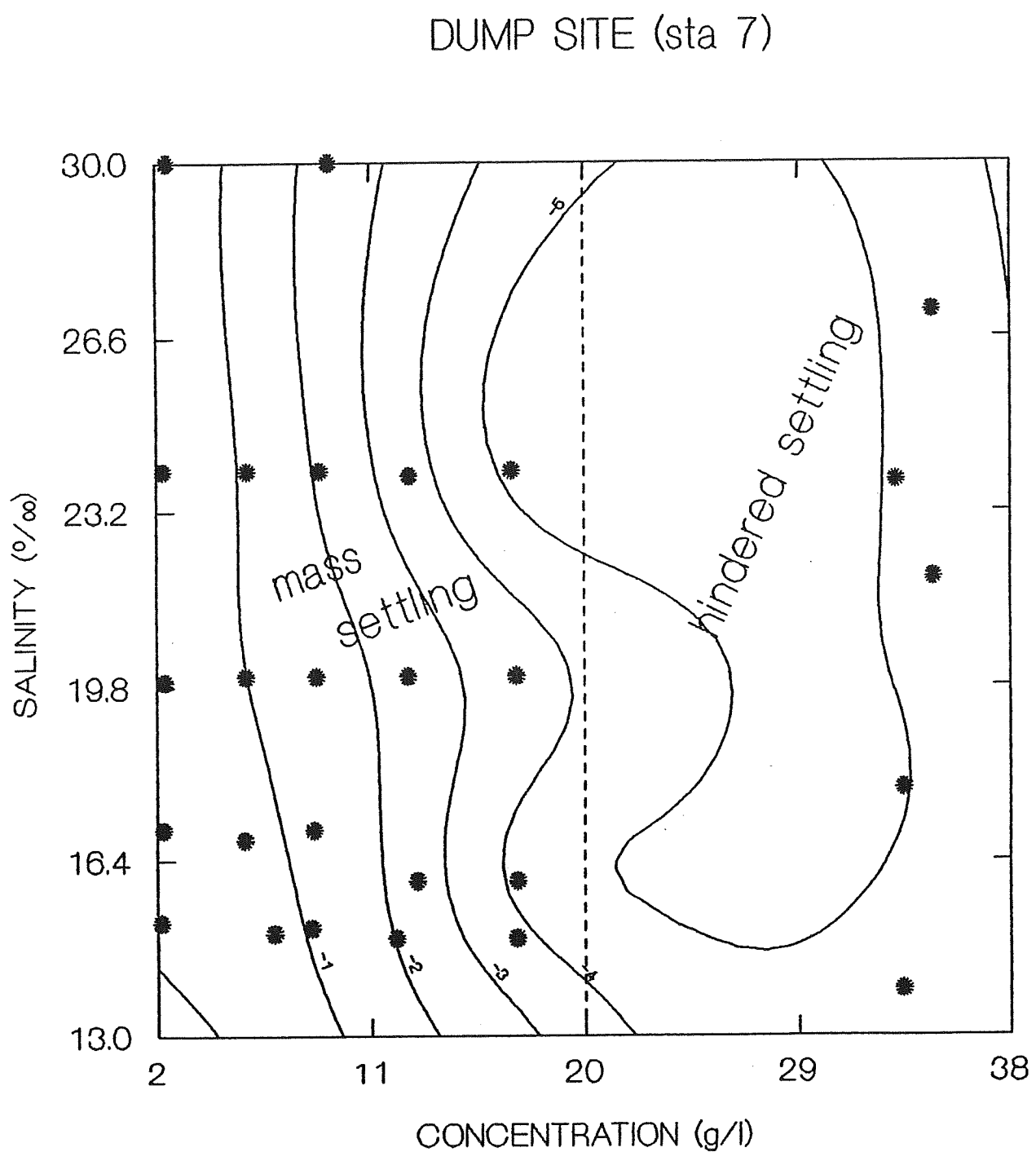


Figure 8. $K_{1\text{lin}}$ as a function of initial suspended sediment concentration and salinity for the Dump Site sample.

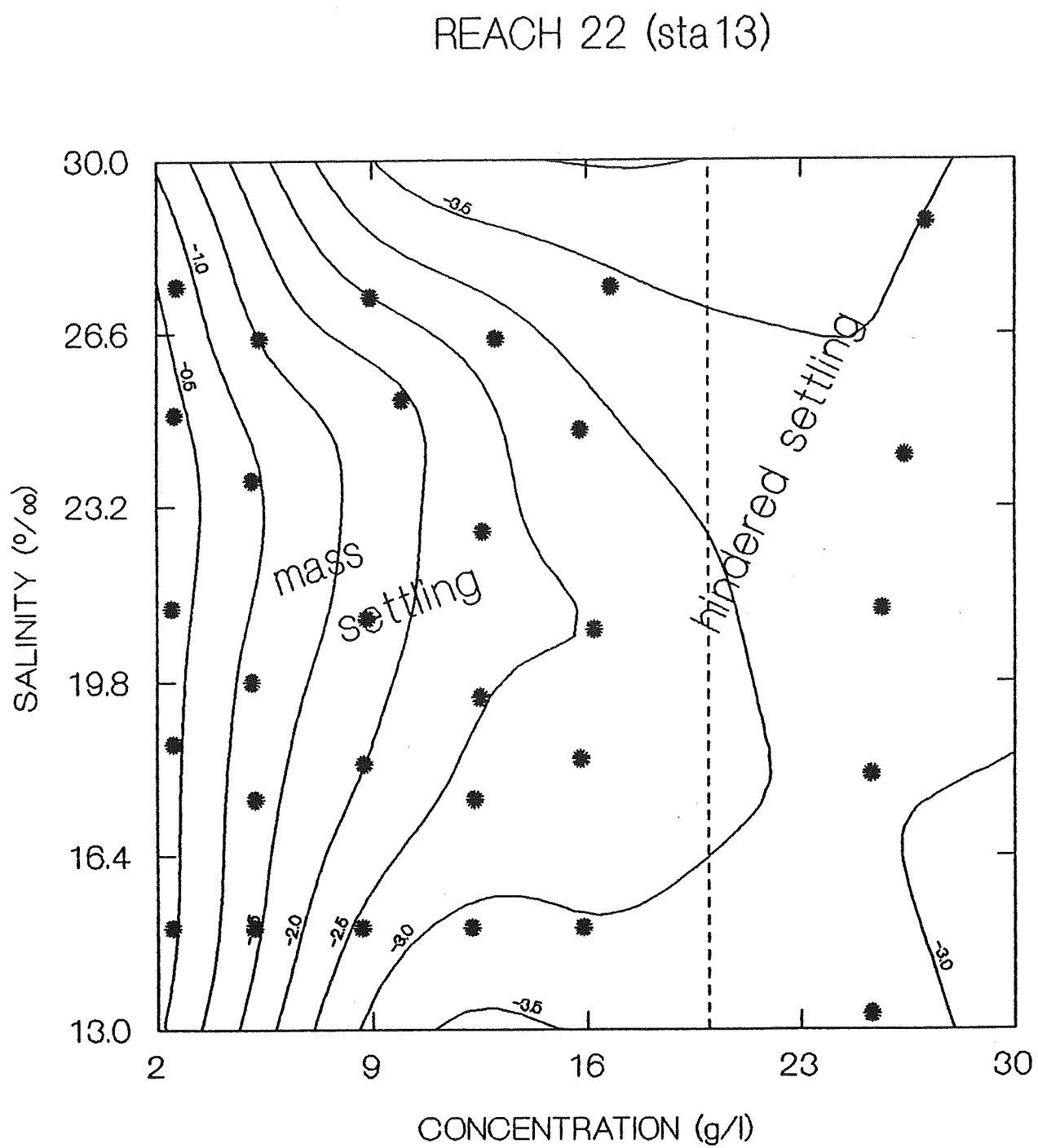


Figure 9. K_{1lin} as a function of initial suspended sediment concentration and salinity for the Reach 22 sample.

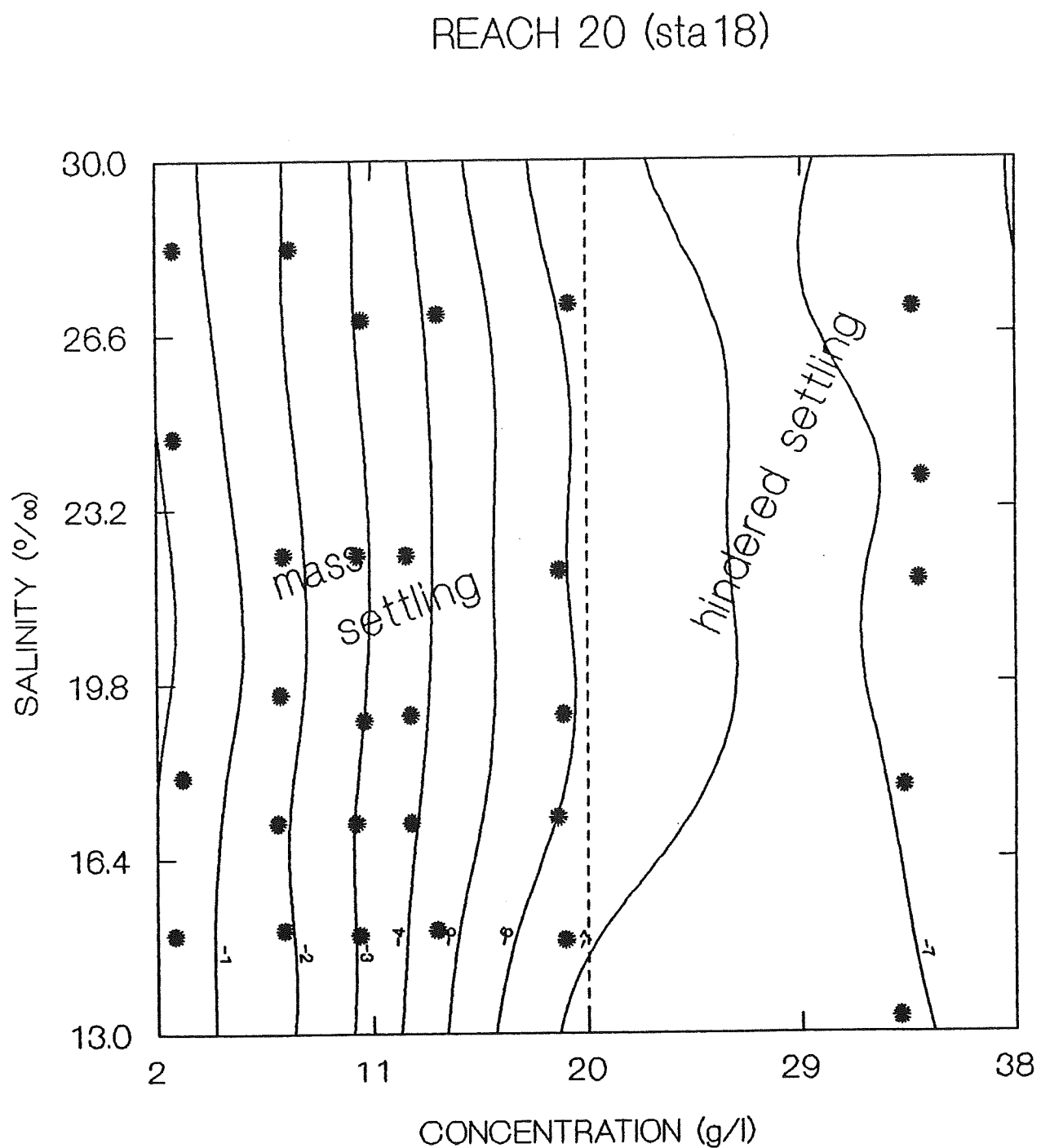
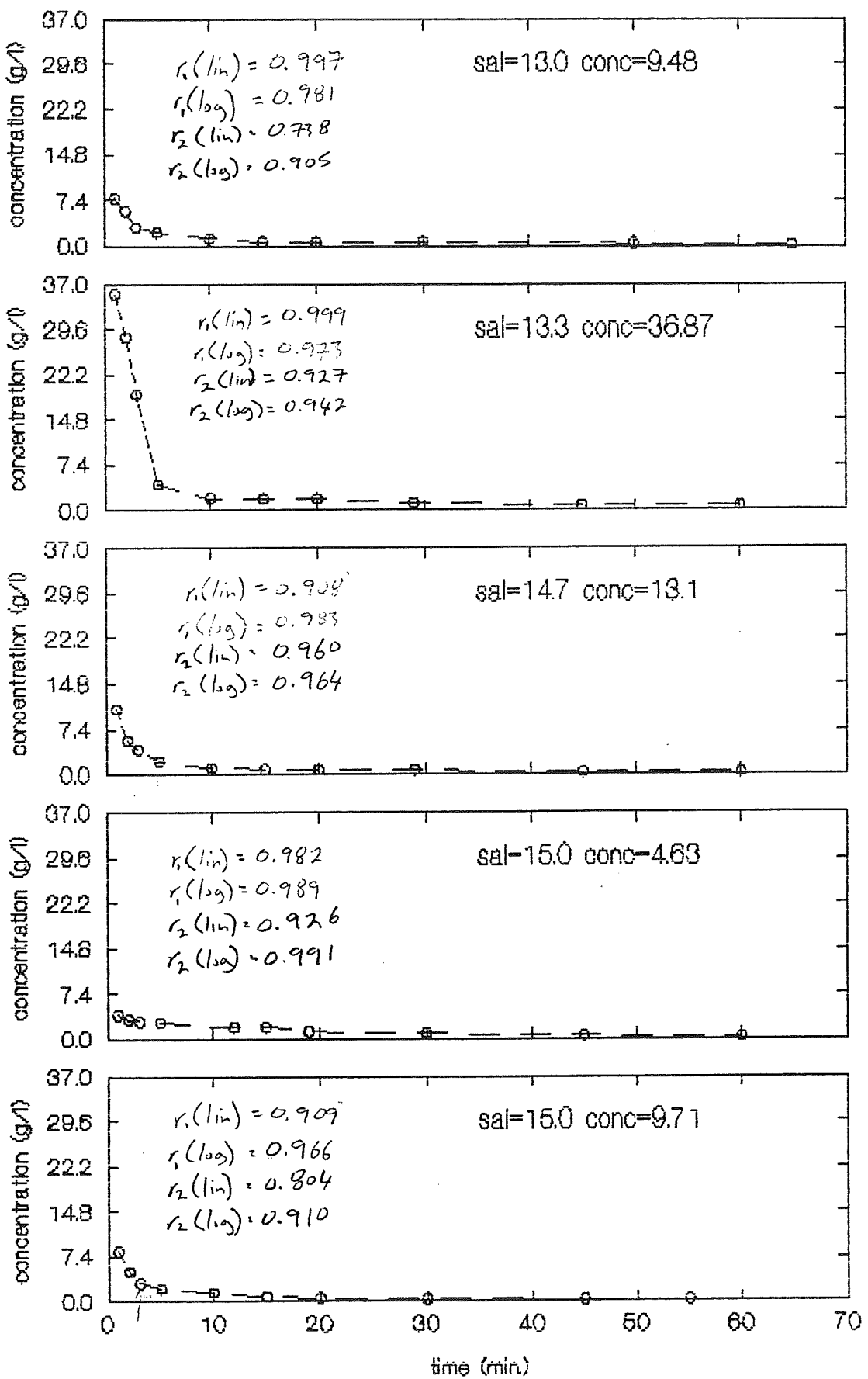


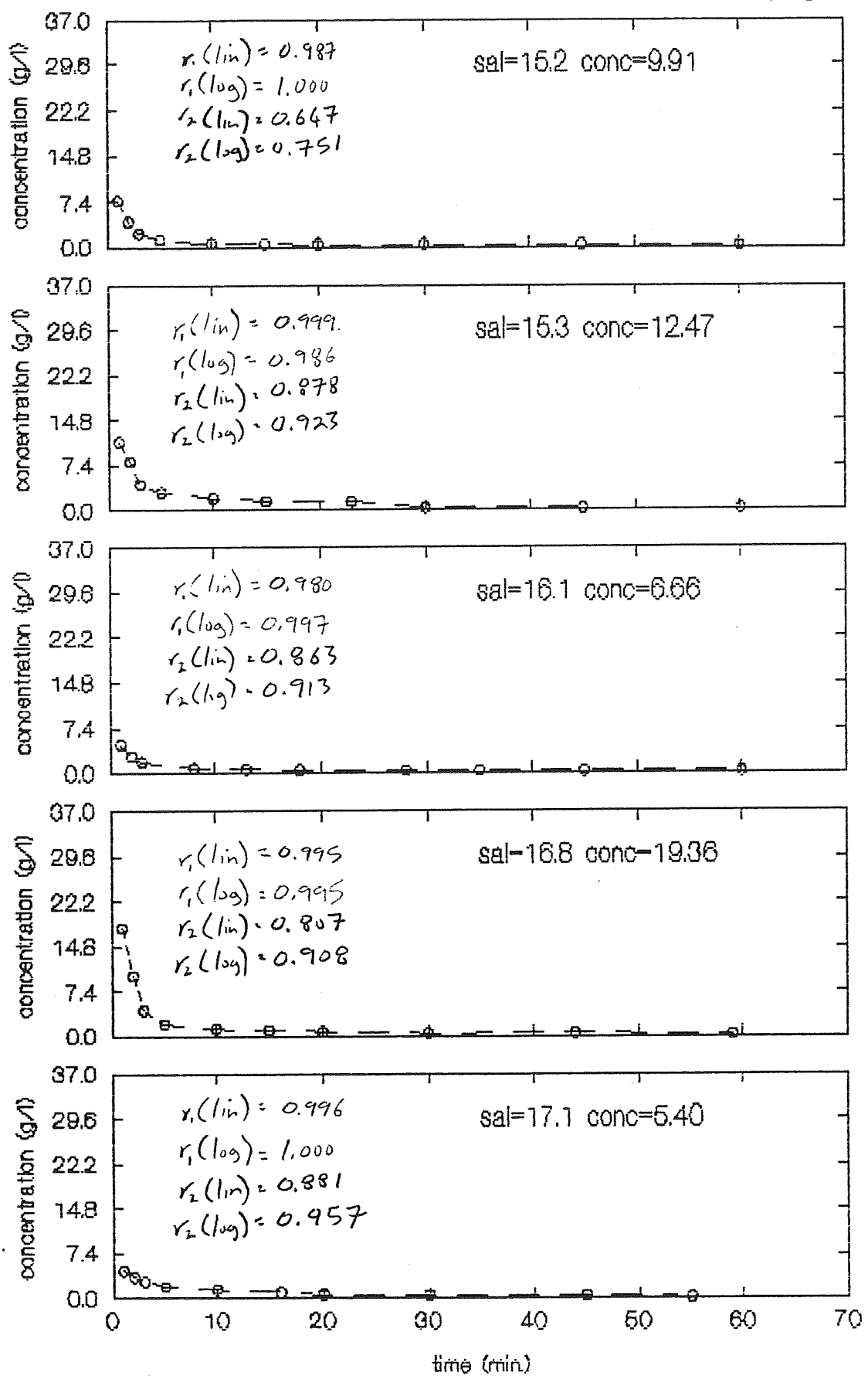
Figure 10. K_{11in} as a function of initial suspended sediment concentration and salinity for the Reach 20 sample.

APPENDIX I

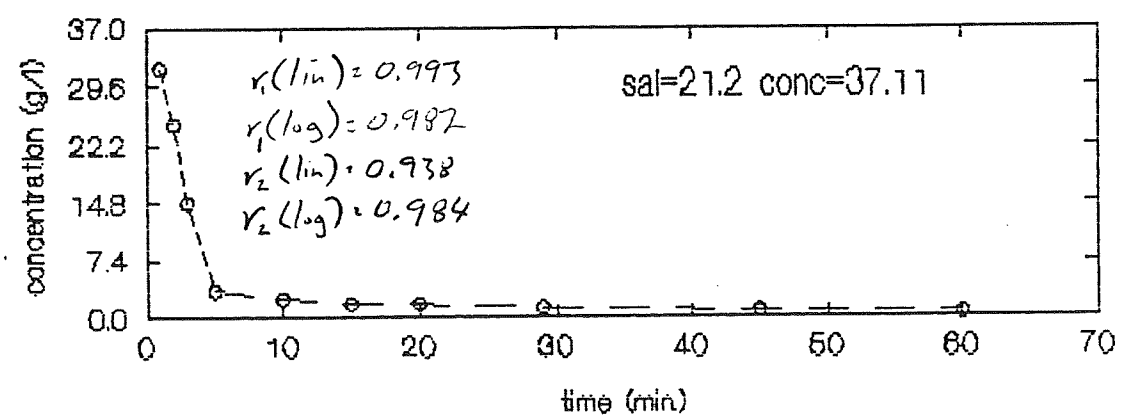
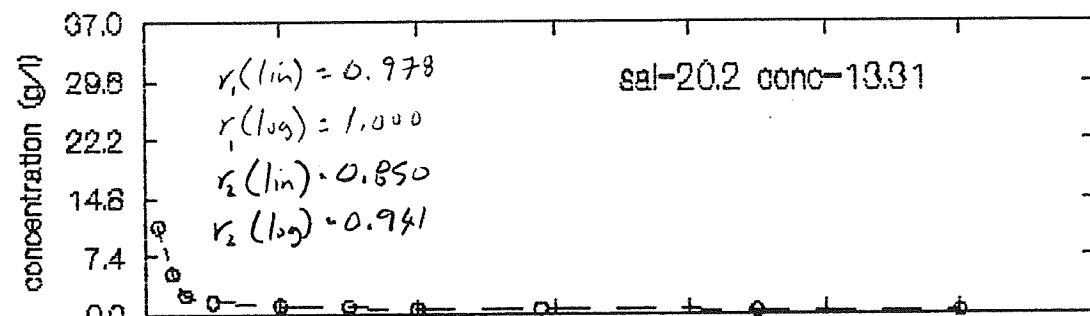
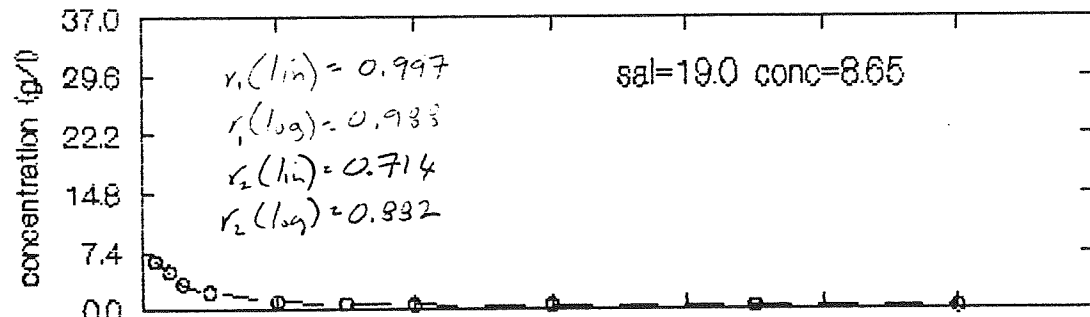
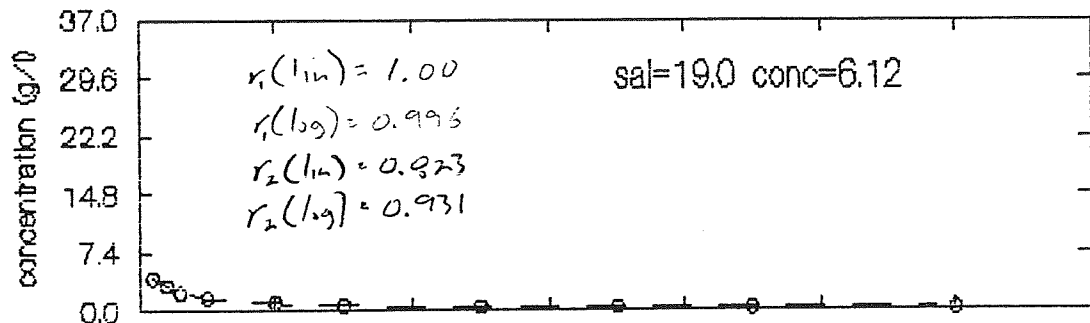
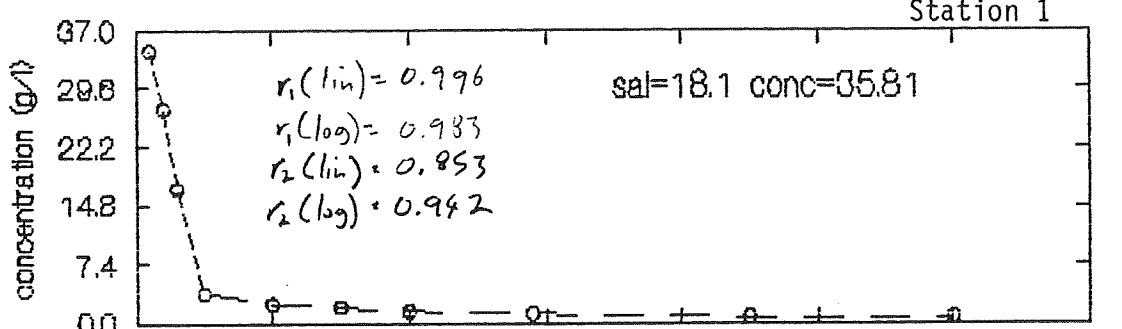
Station 1



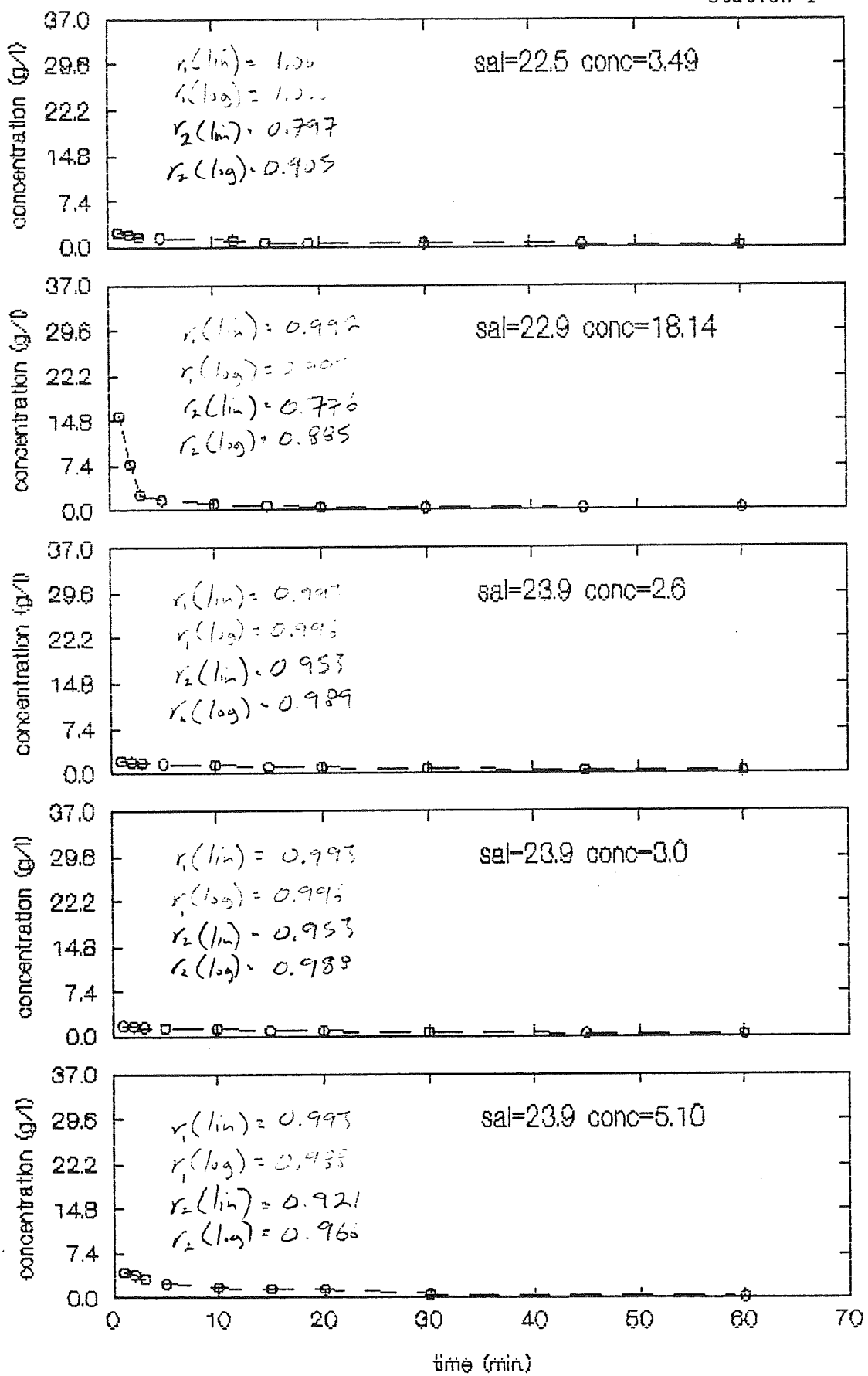
Station 1



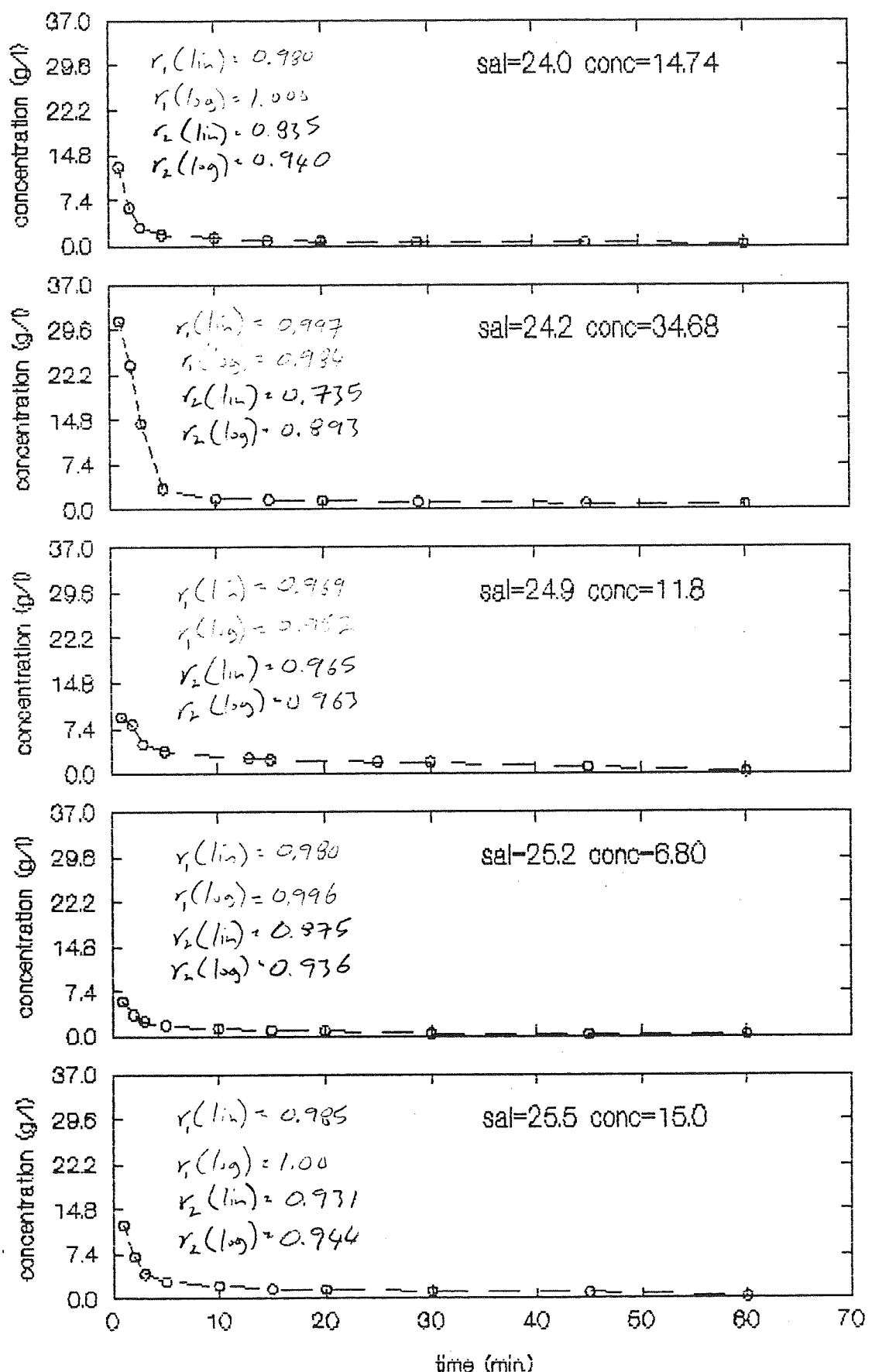
Station 1



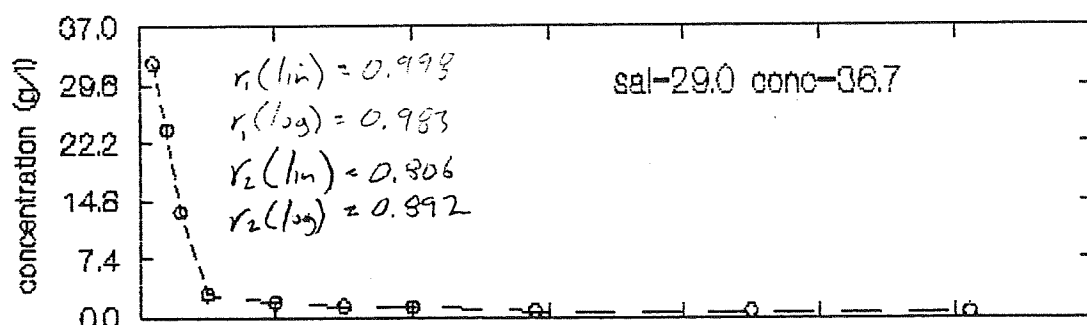
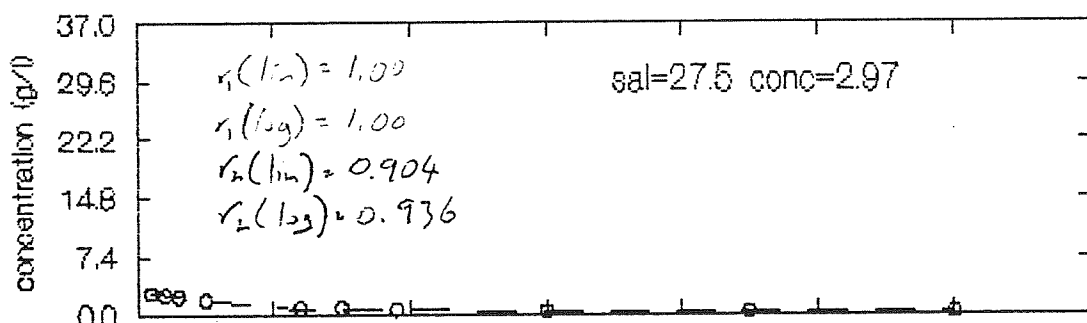
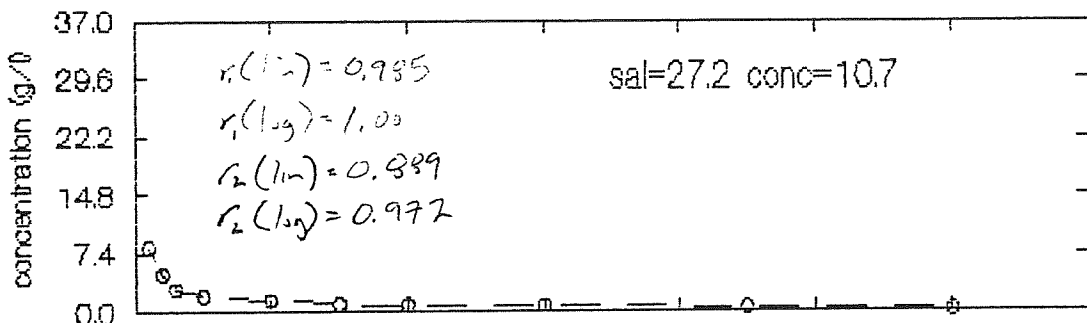
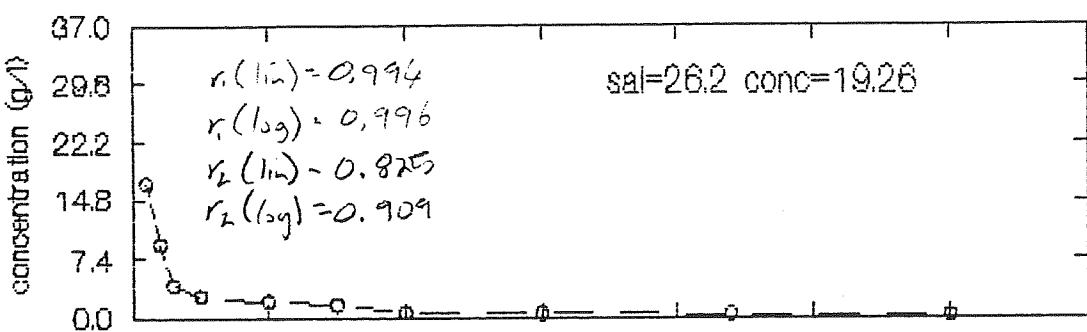
Station 1



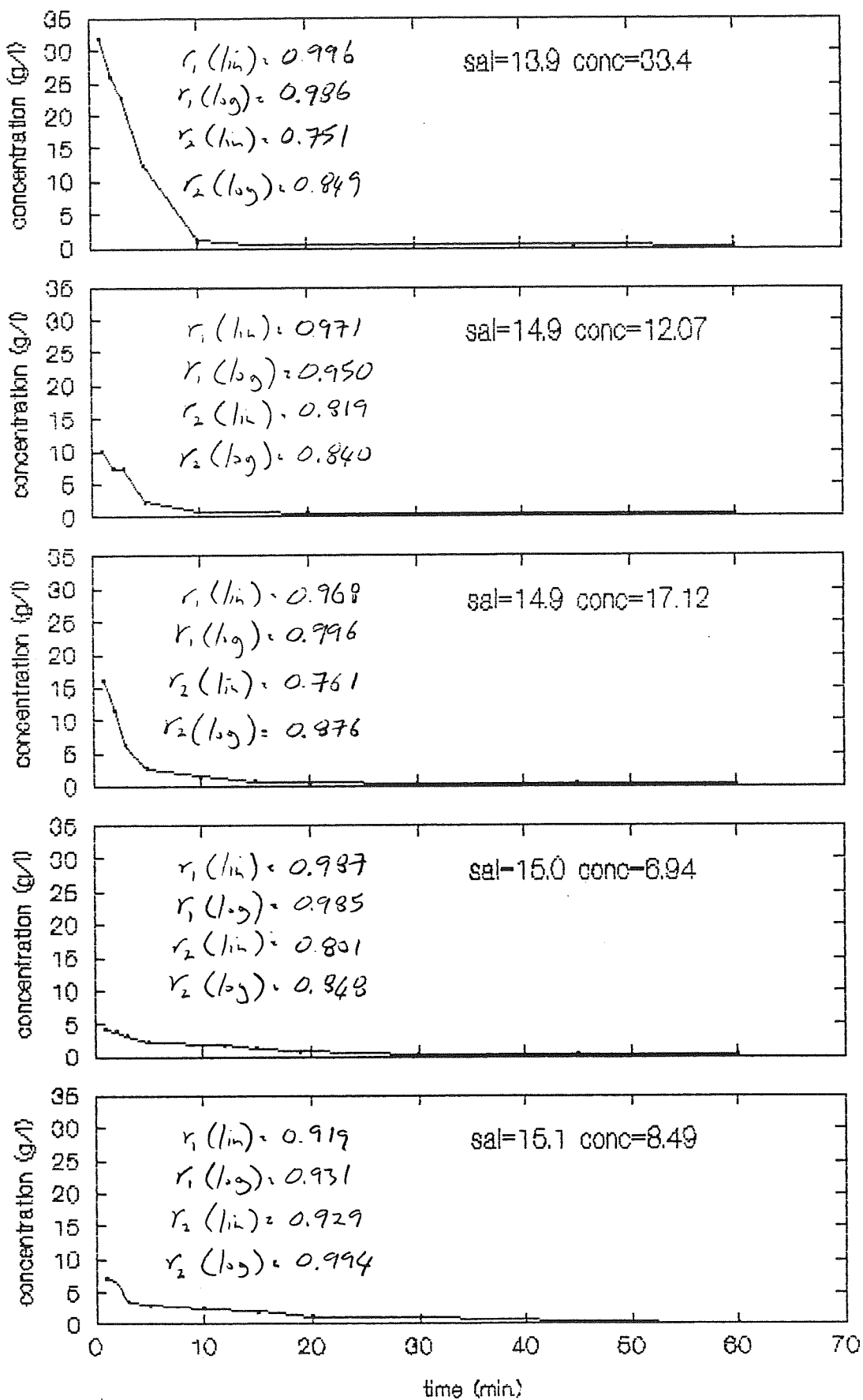
Station 1



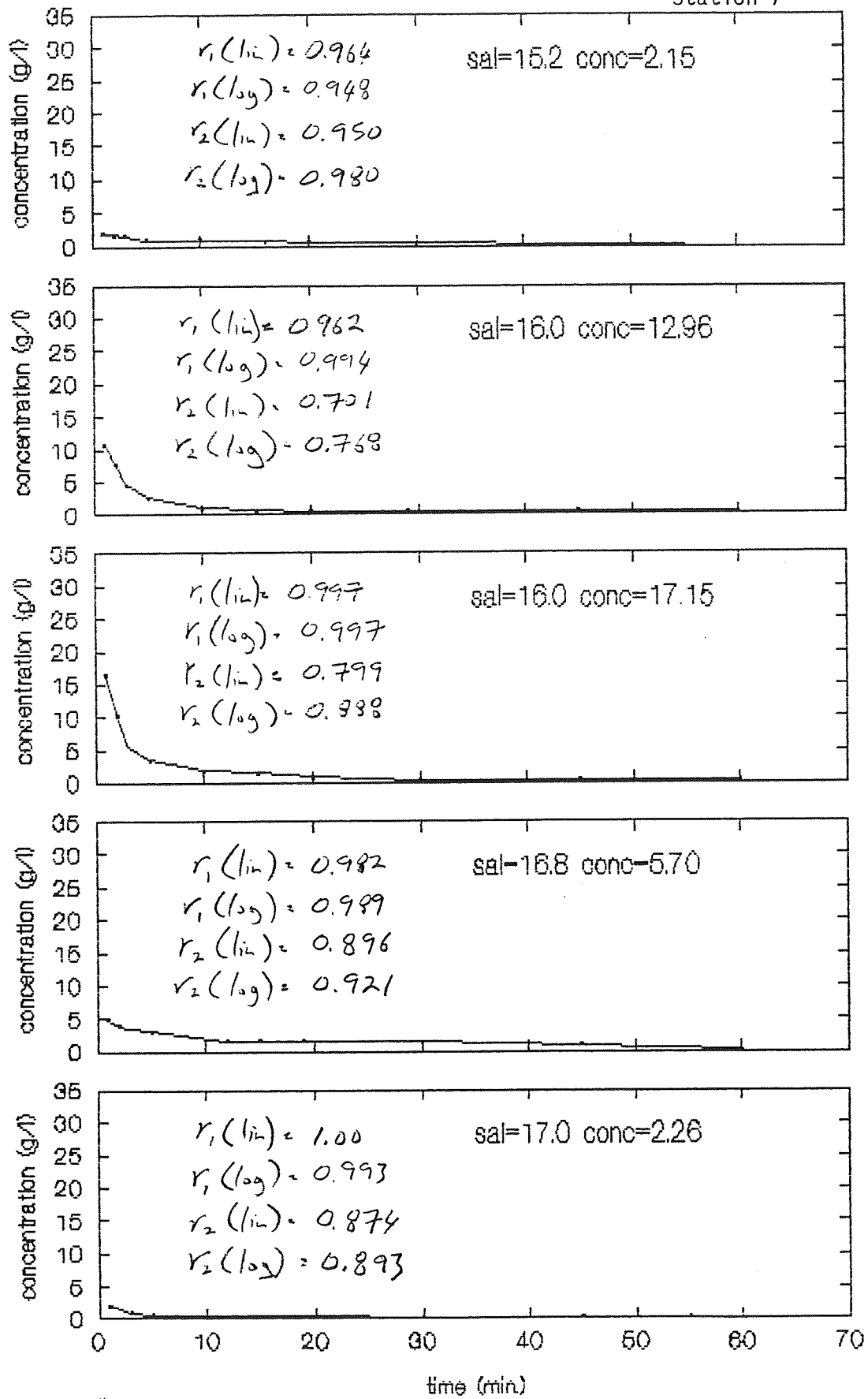
Station 1



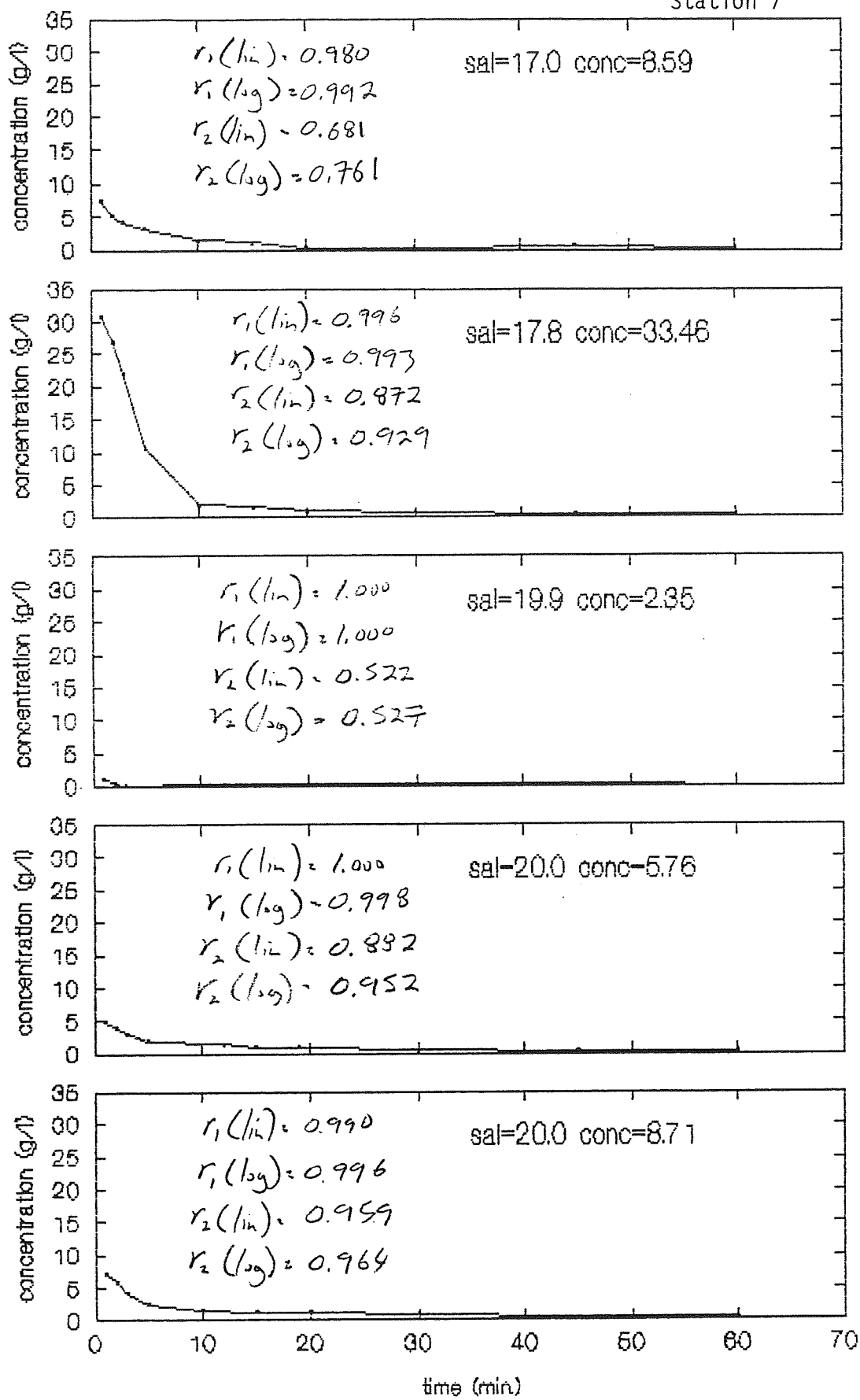
Station 7



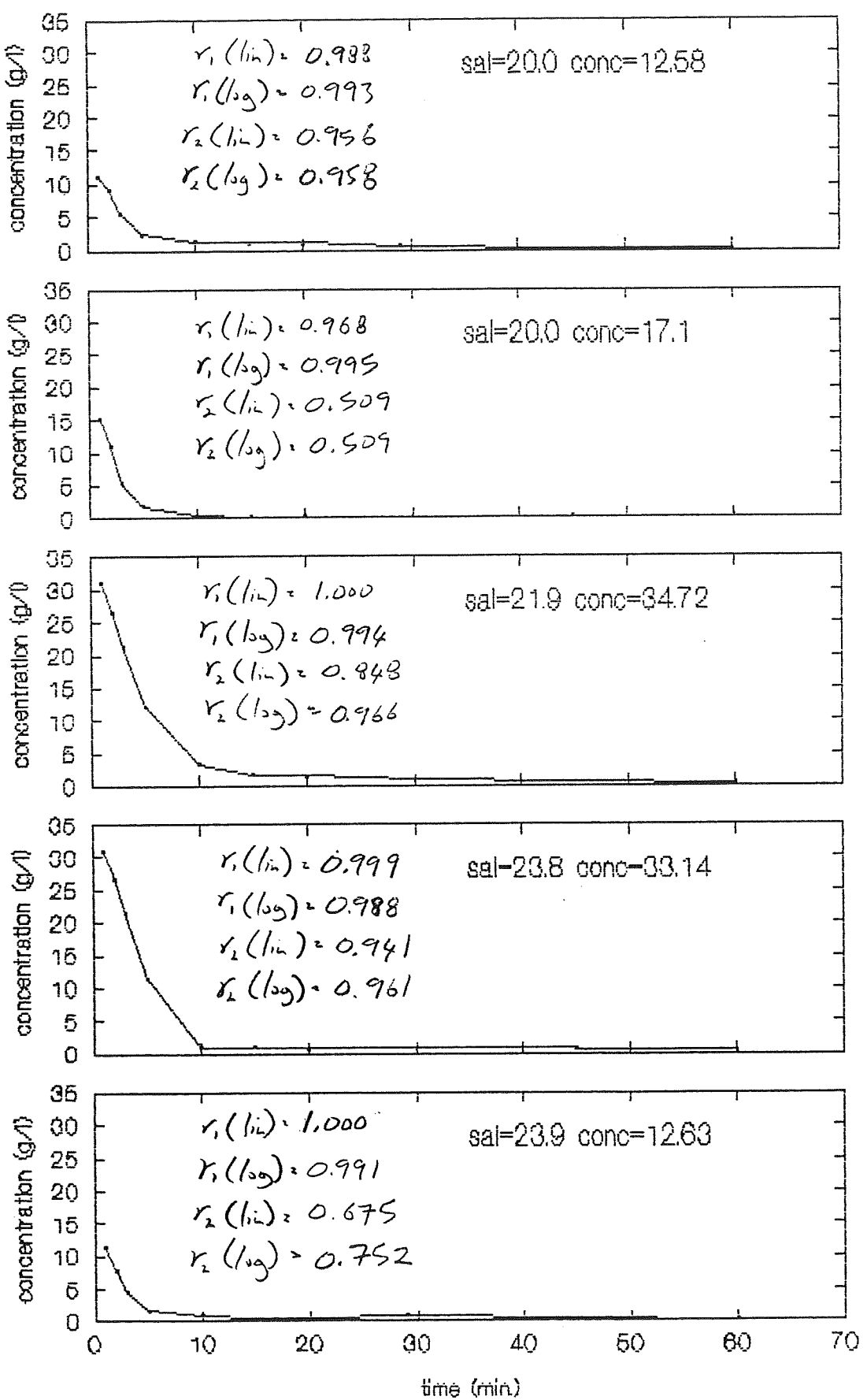
Station 7



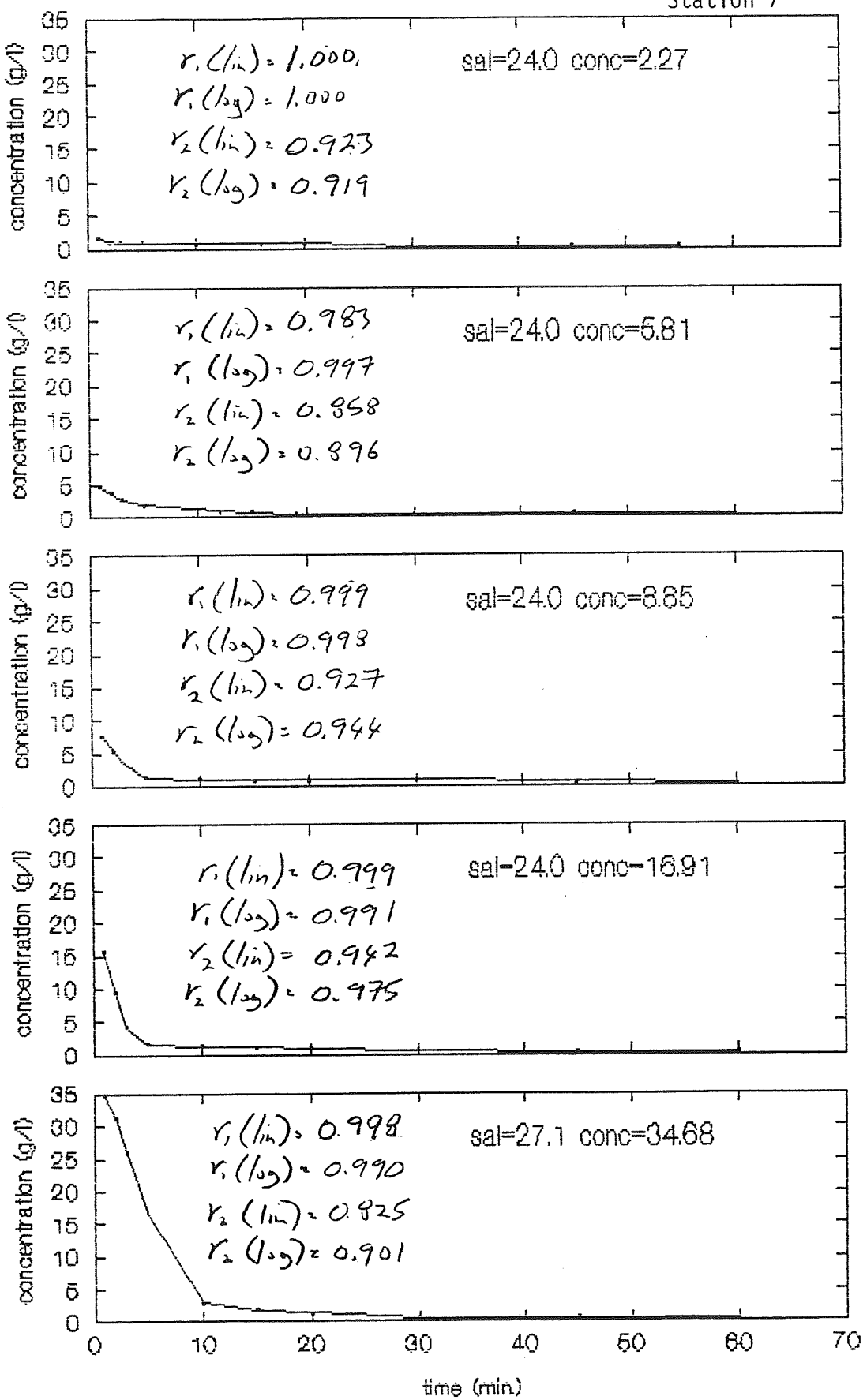
Station 7



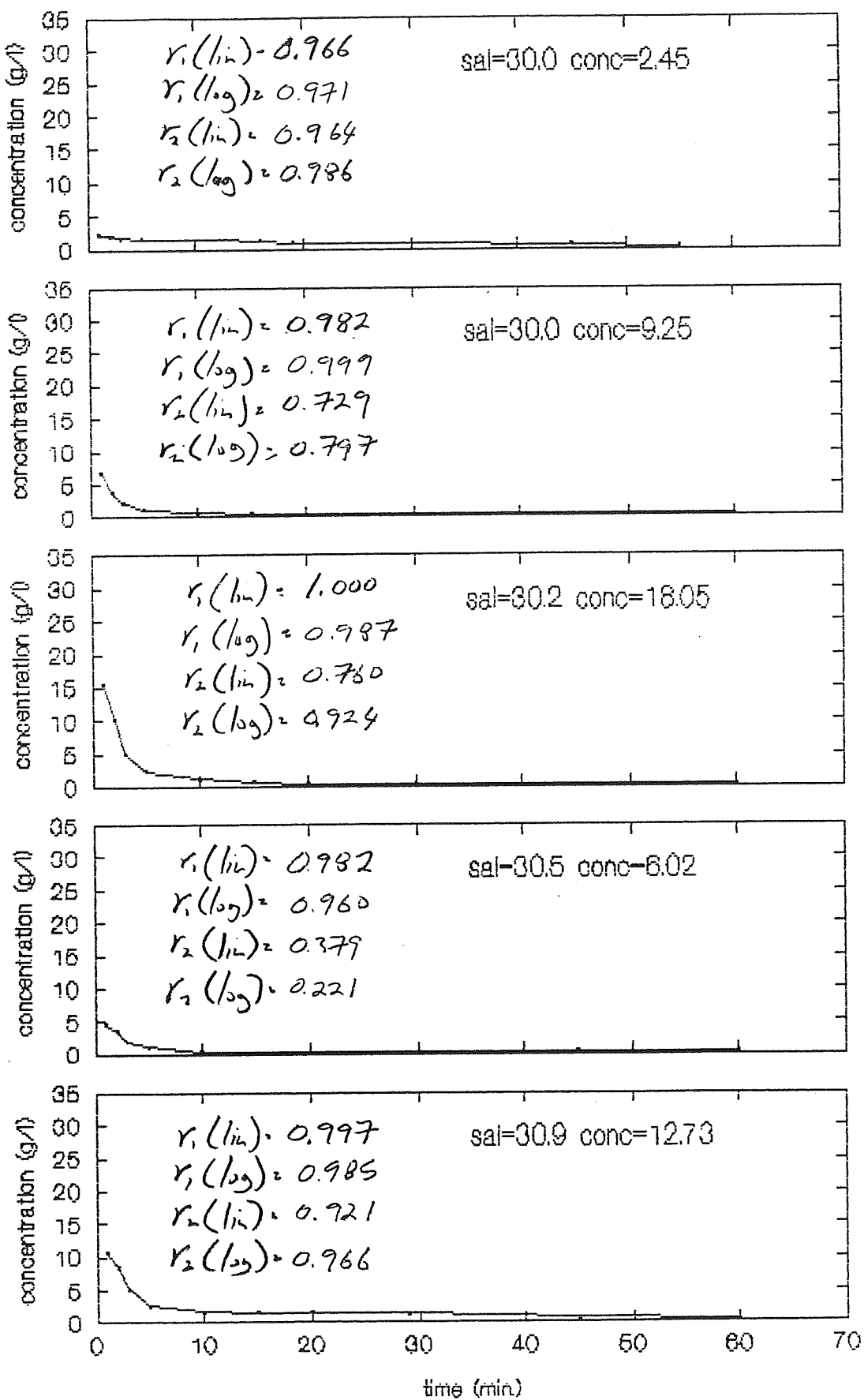
Station 7



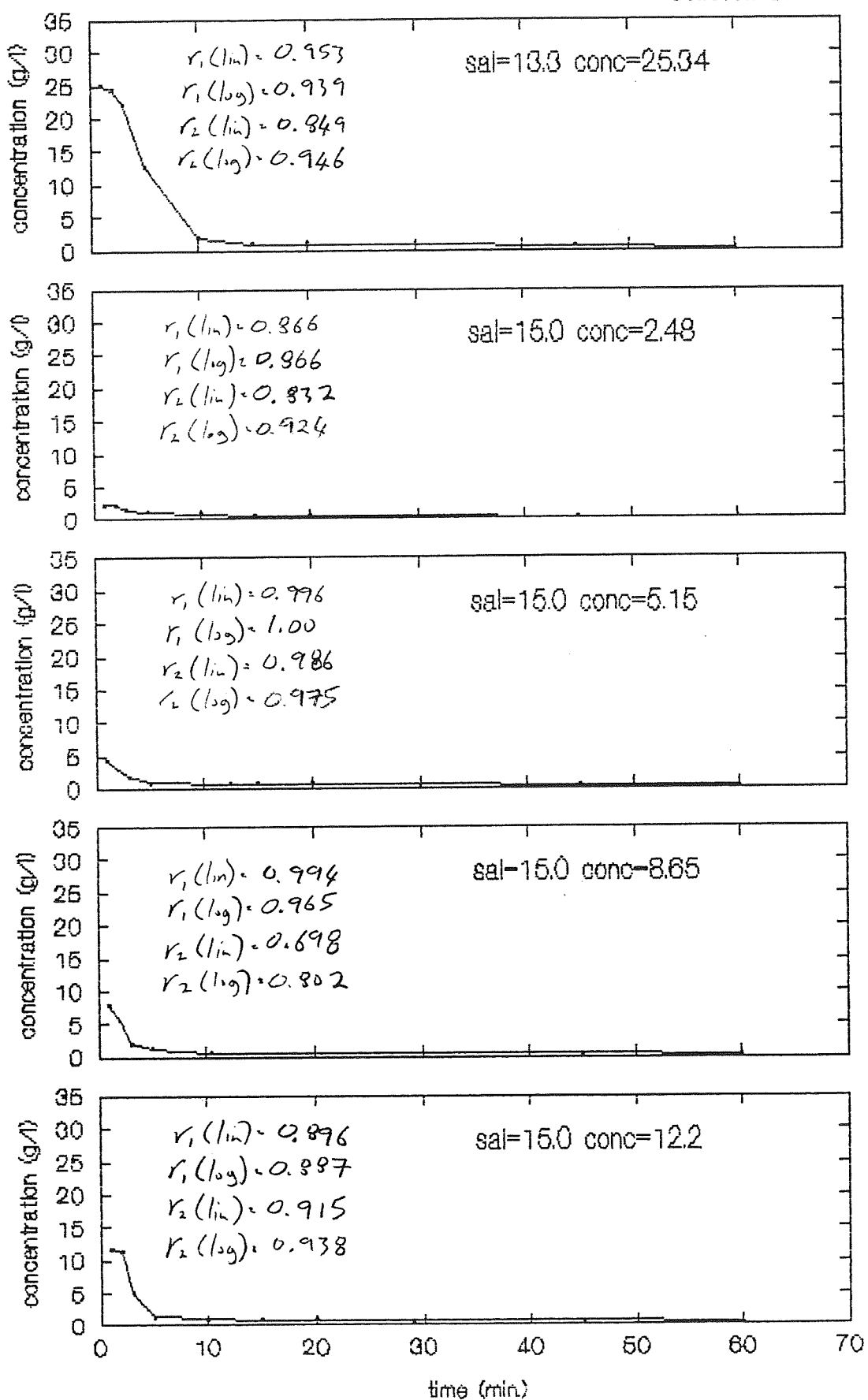
Station 7



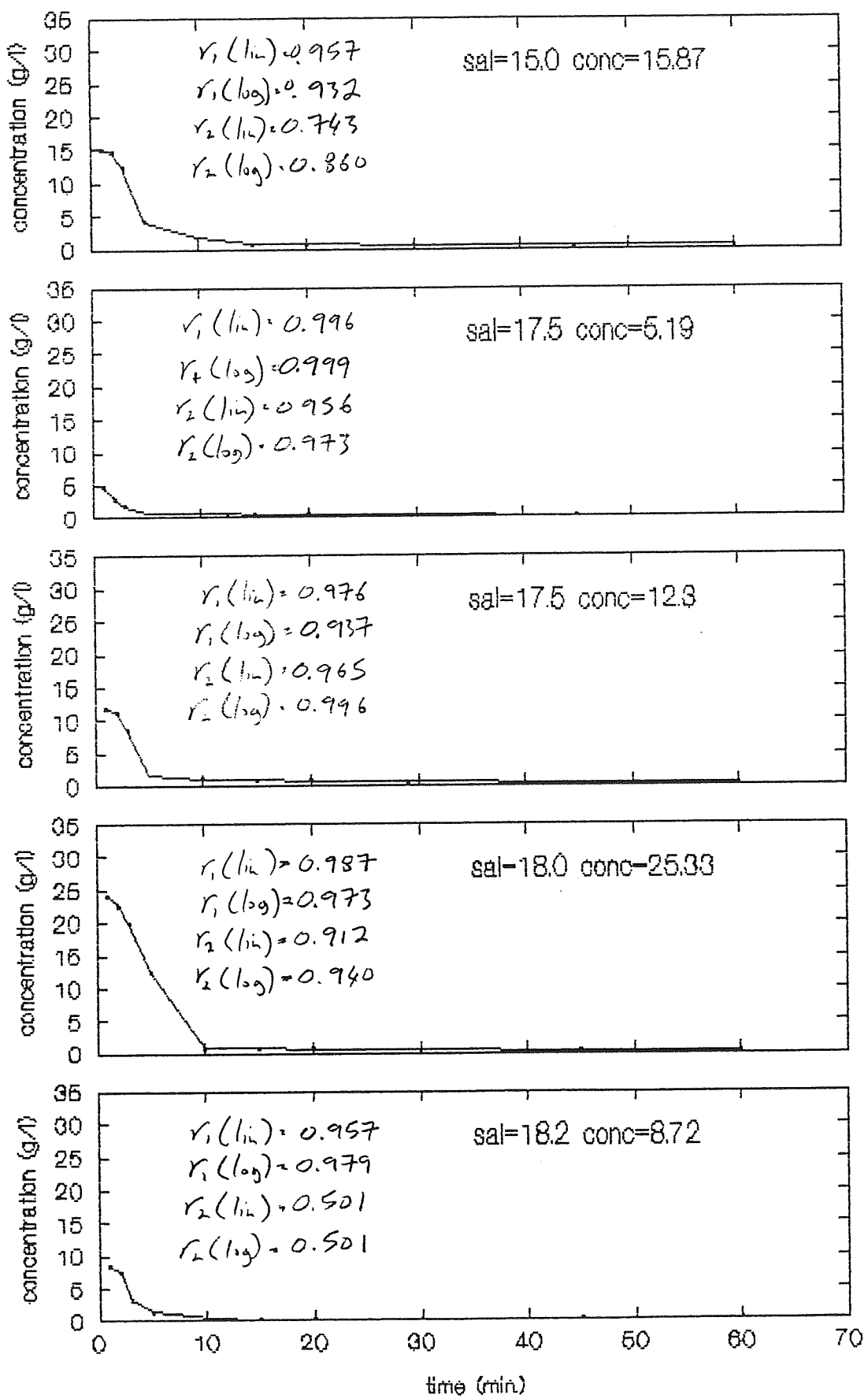
Station 7



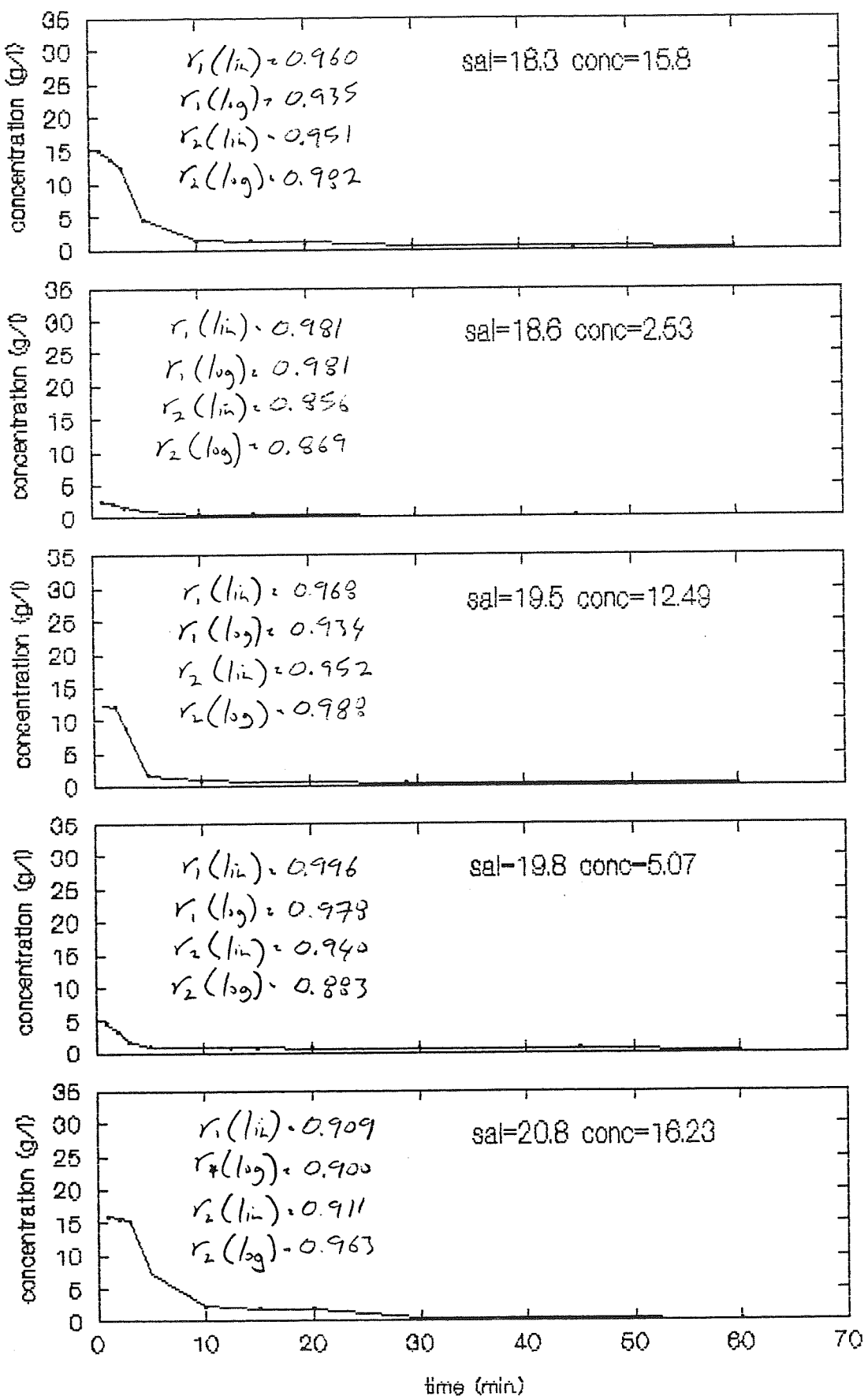
Station 13



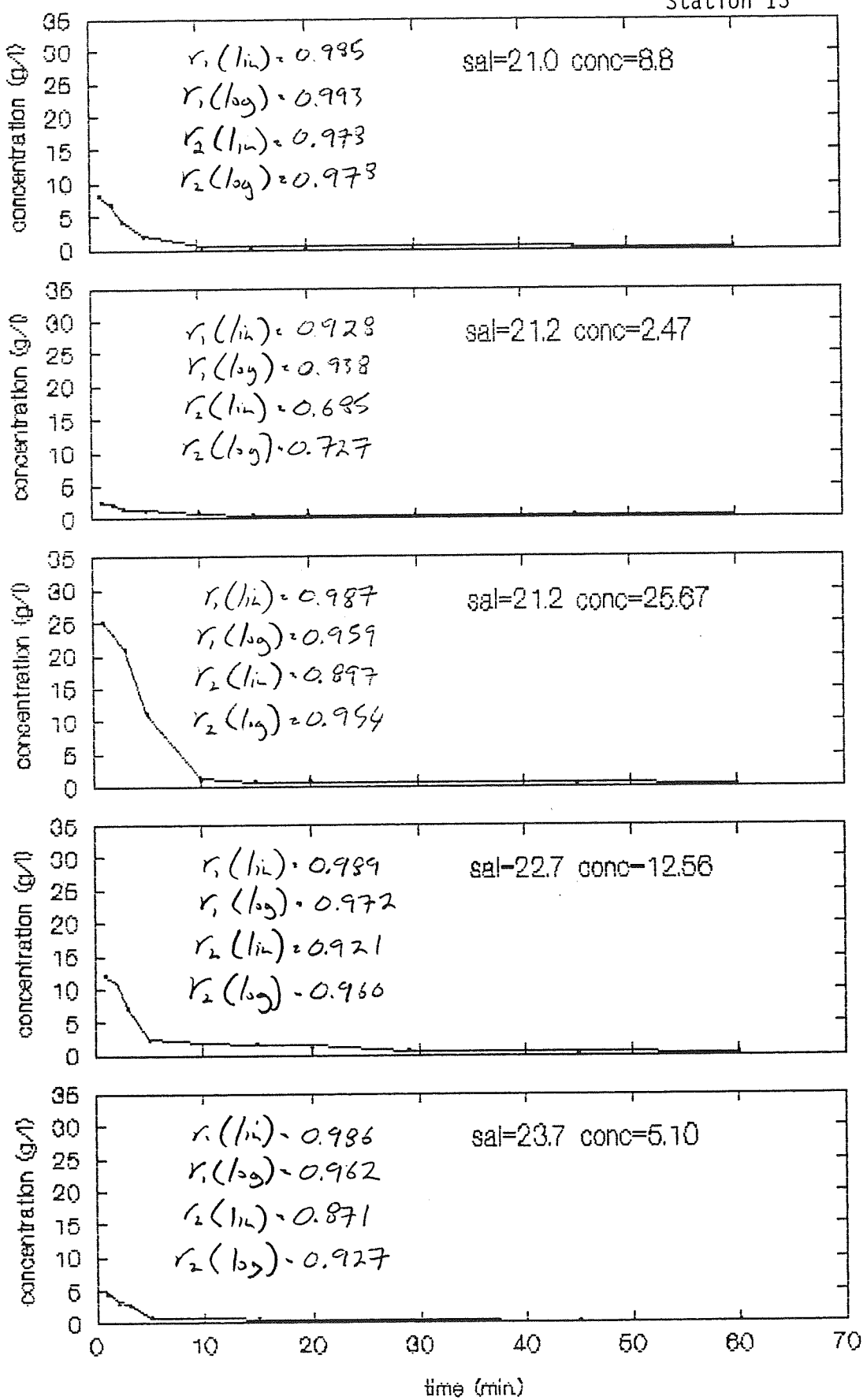
Station 13



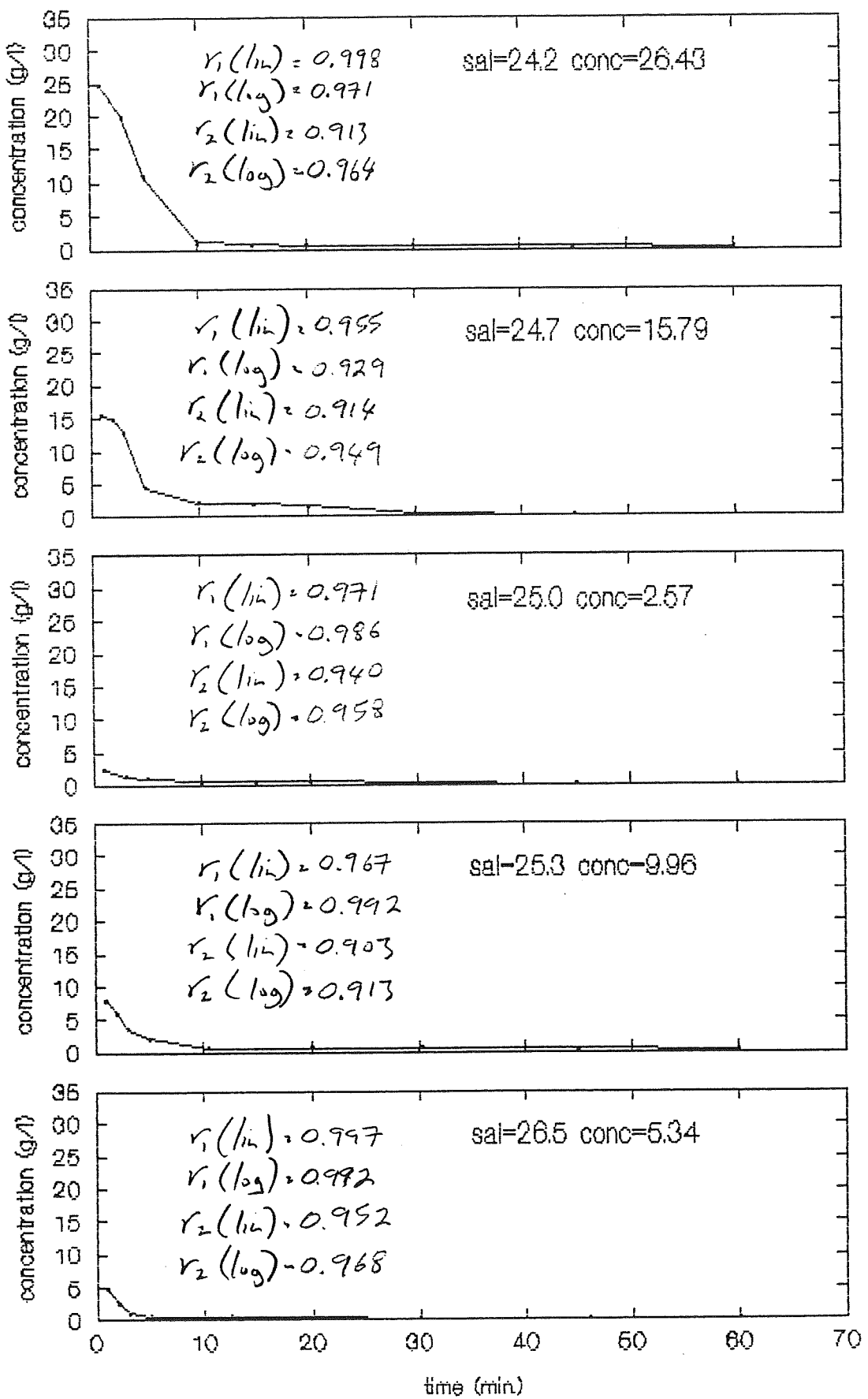
Station 13



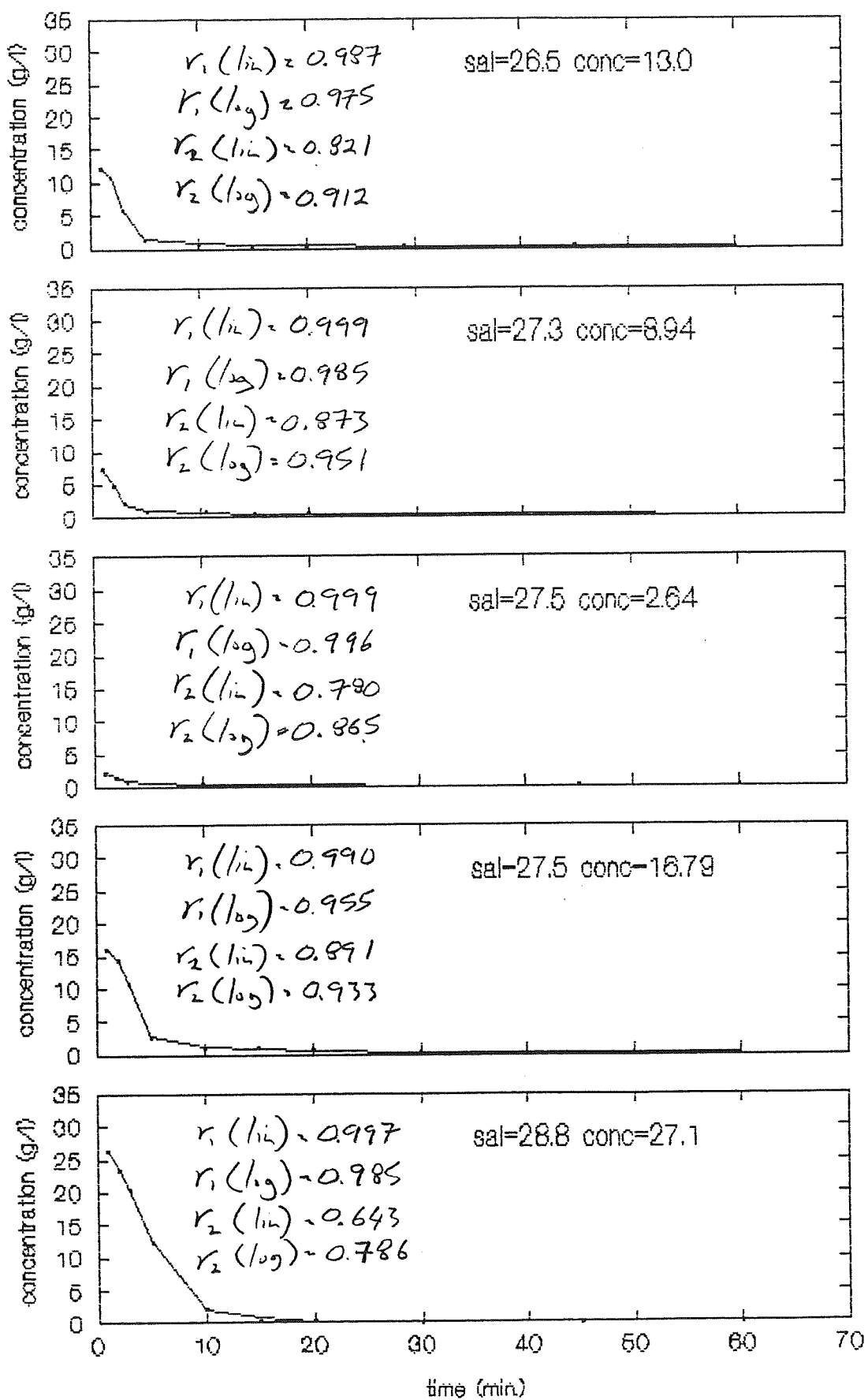
Station 13



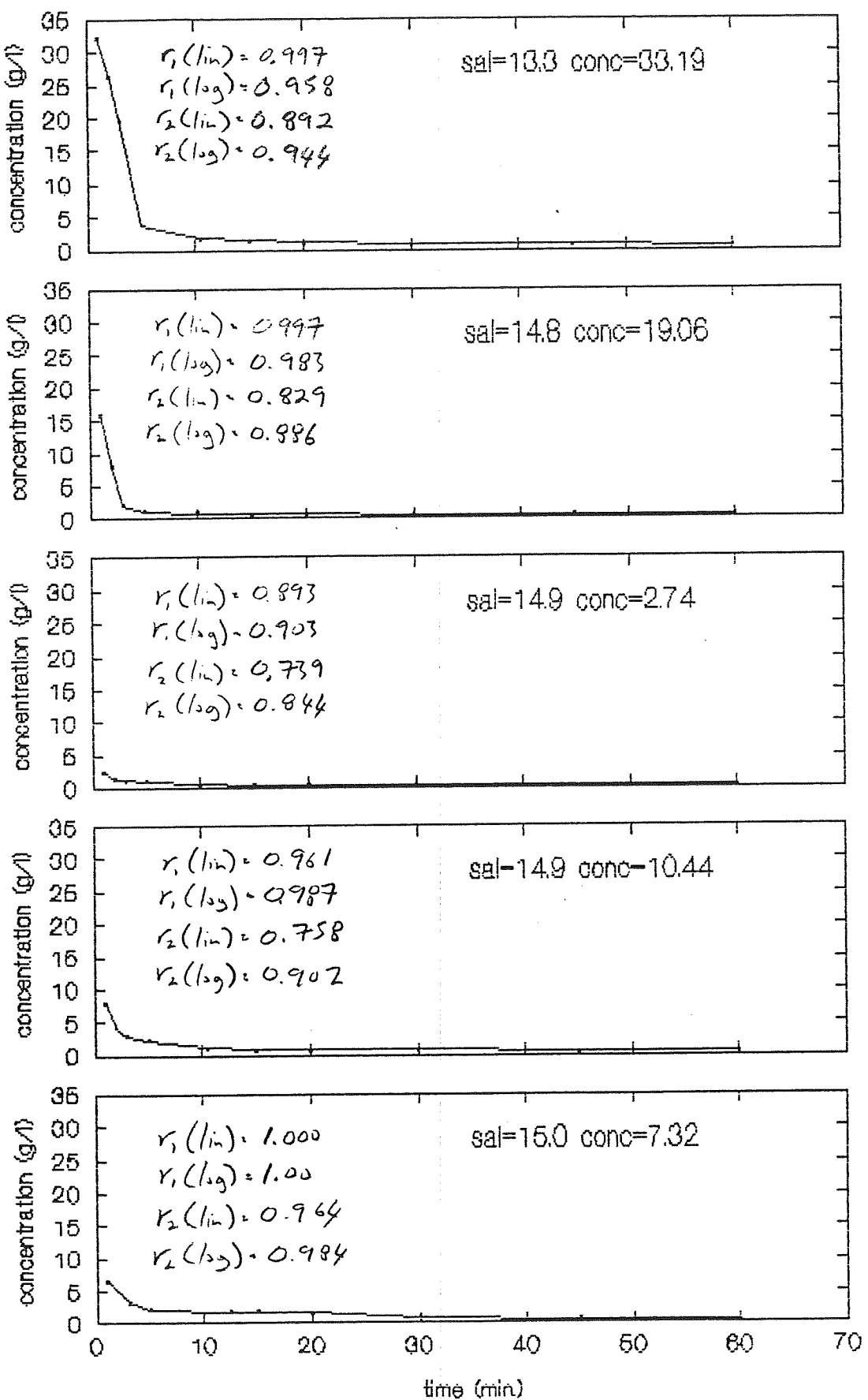
Station 13



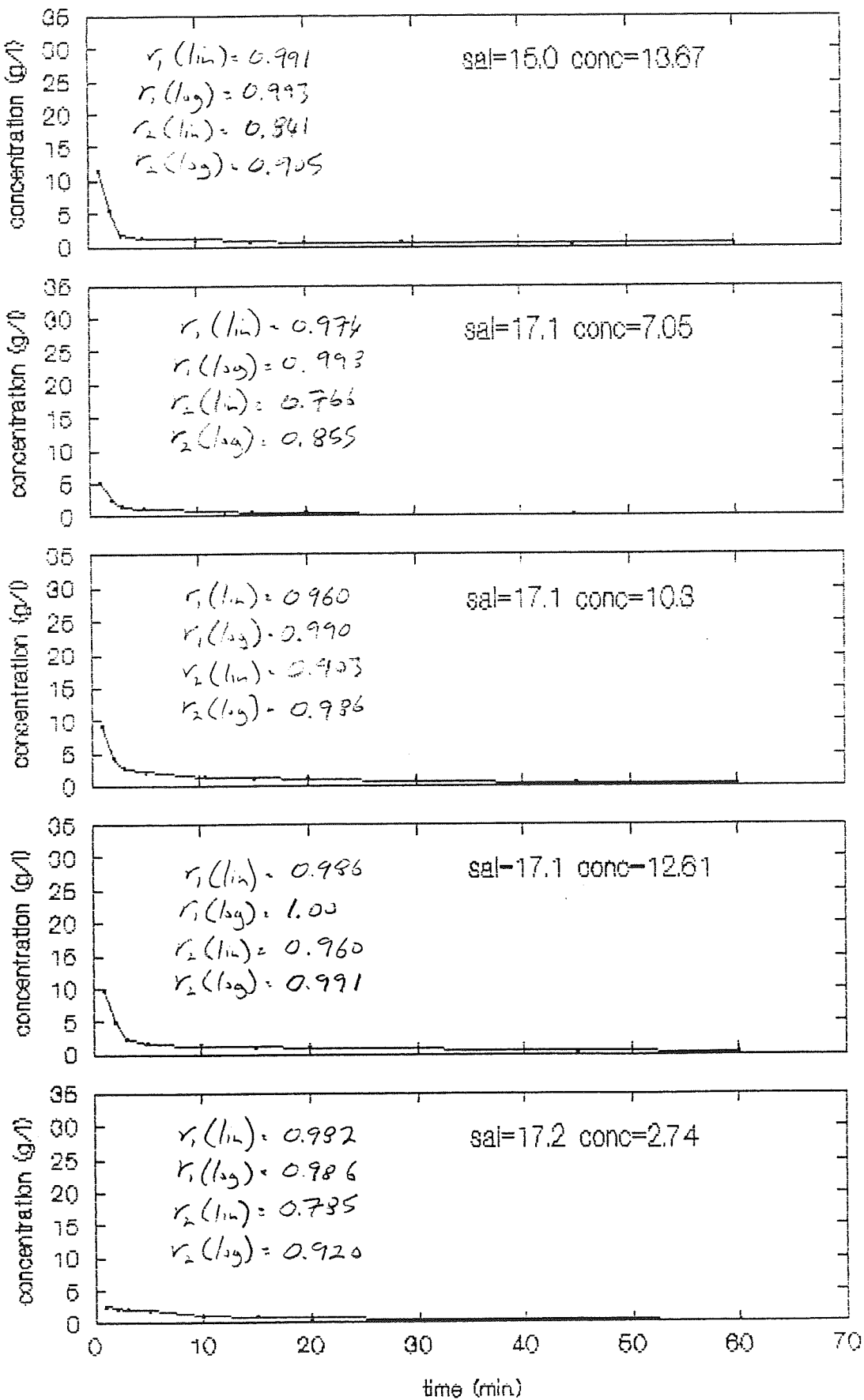
Station 13



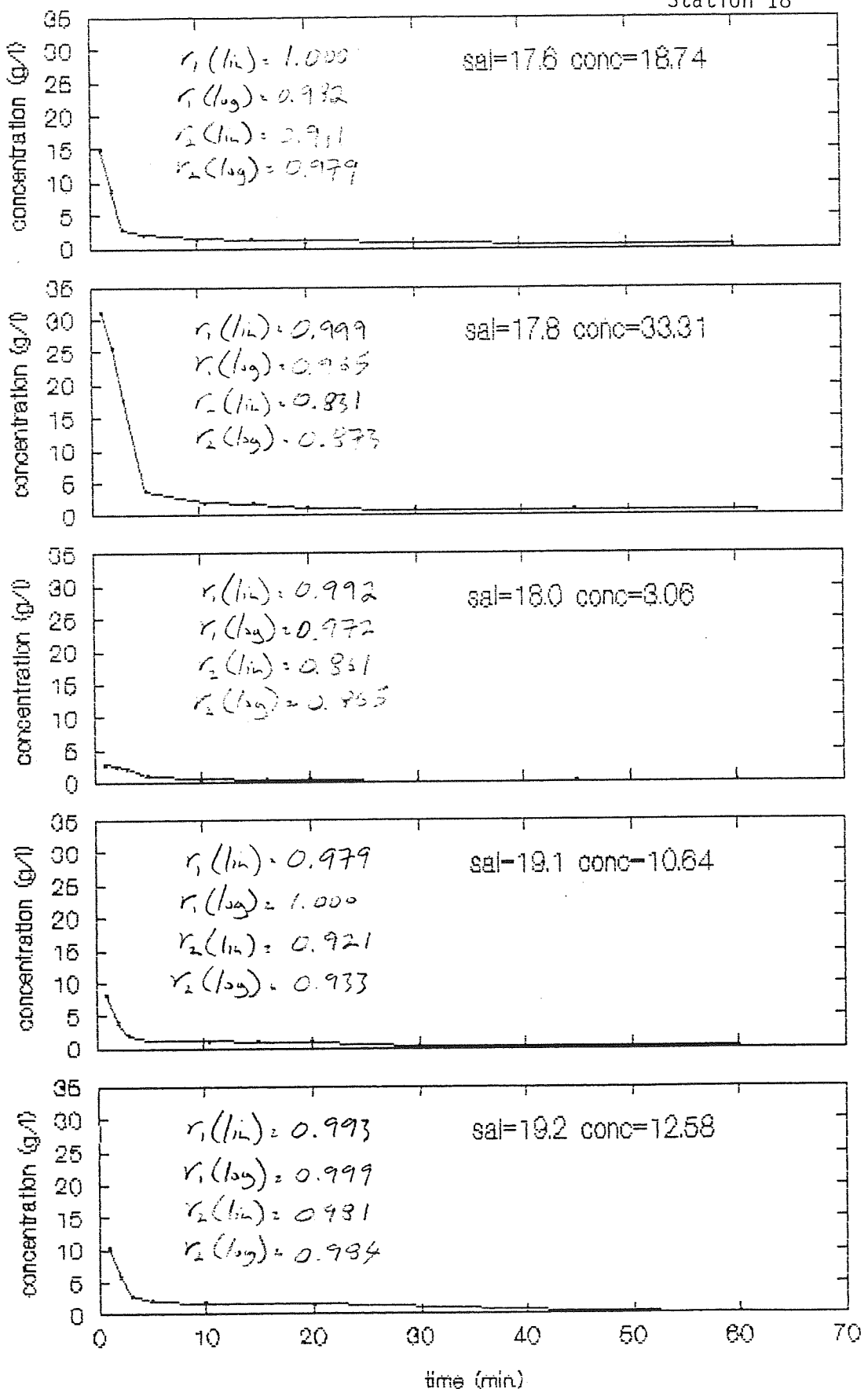
Station 18



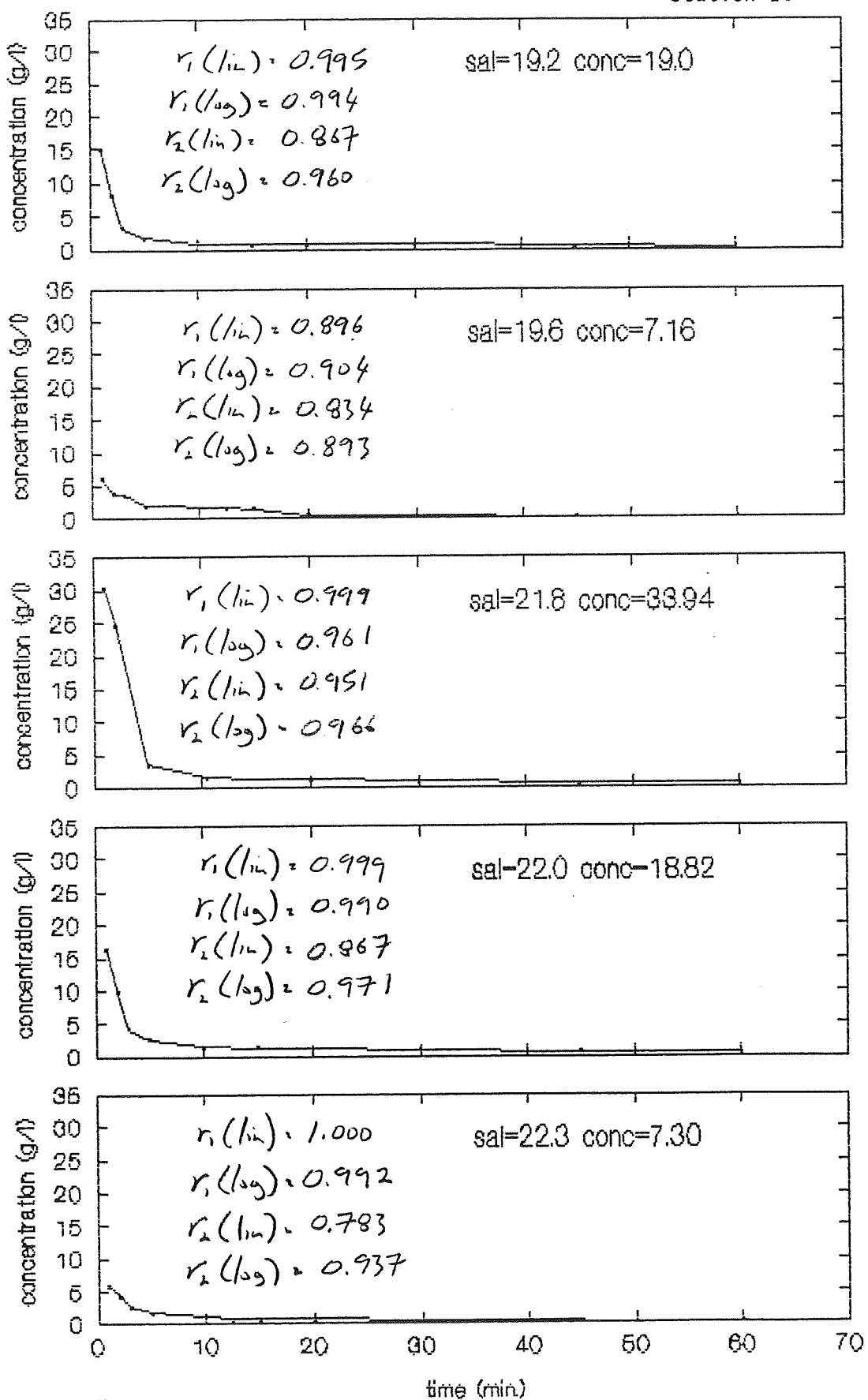
Station 18



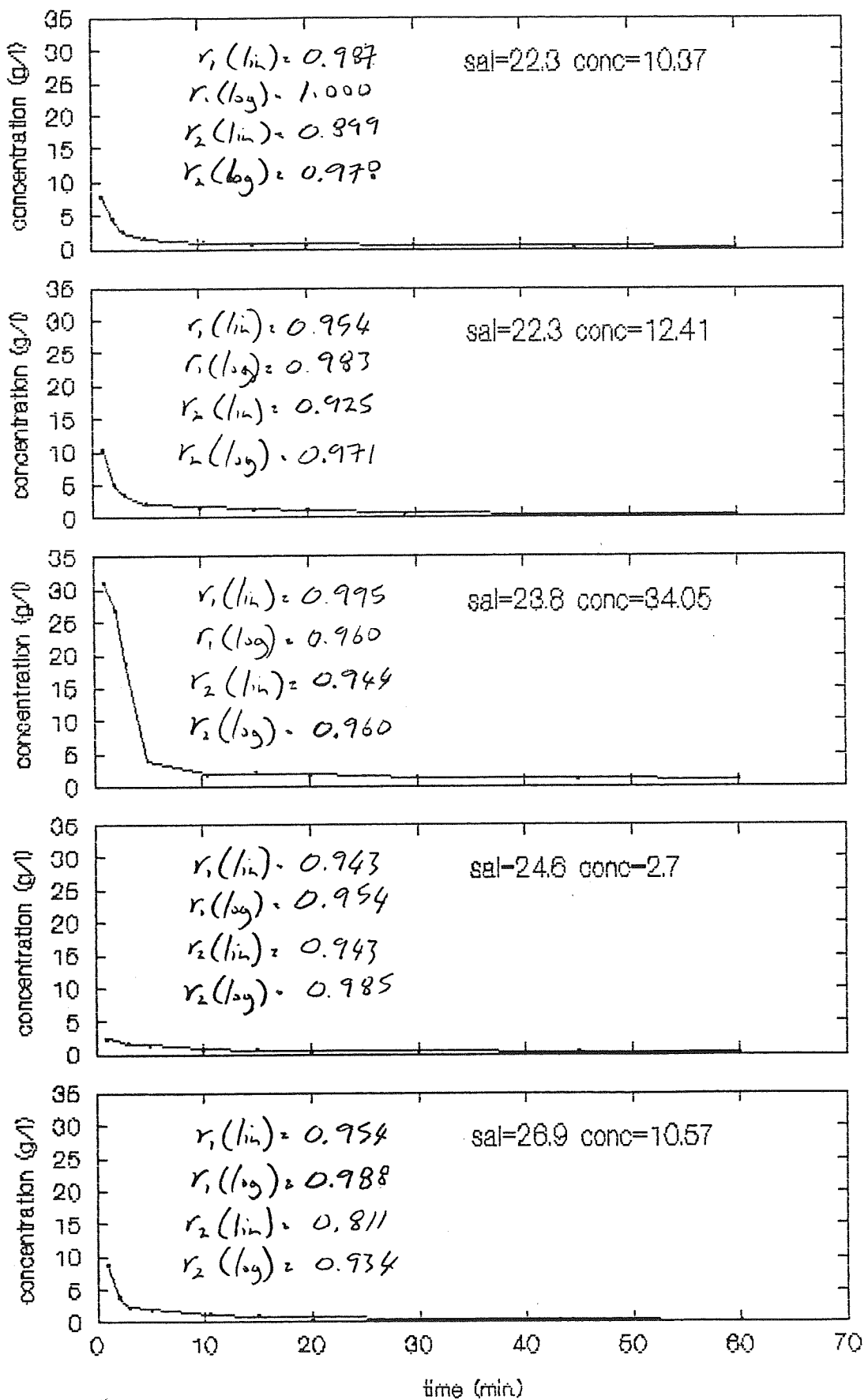
Station 18



Station 18



Station 18



Station 18

